J. Biochem. 2009;146(1)33–41
doi:10.1093/jb/mvp041

High-Sensitivity Analysis of Naturally Occurring Sugar Chains, Using a Novel Fluorescent Linker Molecule

Masaki Sato[1], Yuji Ito[2], Naomichi Arima[3], Masanori Baba[3], Michael Sobel[4], Masahiro Wakao[1] and Yasuo Suda[1,5,*]

[1]Department of Nanostructure and Advanced Materials; [2]Department of Bioengineering, Graduate School of Science and Engineering, Kagoshima University, 1-21-40, Kohrimoto, Kagoshima 890-0065; [3]Center for Chronic Viral Diseases, Graduate School of Medical and Dental Sciences, Kagoshima University, Japan; [4]Department of Surgery, VA Puget Sound HCS and The University of Washington School of Medicine, Seattle, WA, USA; and [5]SUDx-Biotec Corp., 1-42-1, Shiroyama, Kagoshima, 890-0013, Japan

Received February 16, 2009; accepted February 26, 2009; published online March 6, 2009

To analyse the binding of sugar chains to proteins, viruses and cells, the surface plasmon resonance (SPR) technique is very convenient and effective because it is a real-time, non-destructive detection system. Key to this method is linker compounds for immobilization of the sugar chains to the gold-coated chip for SPR. Also, well-designed fluorescent labelling reagents are essential when analysing the structure of trace amounts of sugar chains derived from natural sources, such as glycoproteins on the surface of specific cells. In this report, we developed a novel linker molecule, named 'f-mono', which has both of these properties: simple immobilization chemistry and a fluorescent label. Since the molecule contains a 2,5-diaminopyridyl group and a thioctic acid group, conjugation with sugar chains can be achieved using the well-established reductive amination reaction. This conjugate of sugar chain and fluorescent linker (fluorescent ligand-conjugate, FLC) has fluorescent properties (ex. 335 nm, em. 380 nm), and as little as 1 μg of FLC can be easily purified using HPLC with a fluorescent detector. MS and MS/MS analysis of the FLC is also possible. As a +2 Da larger MS peak ($[M+H+2]^+$ ion) was always associated with the theoretical MS peak ($[M+H]^+$) (due to the reduction of the thioctic acid moiety), the MS peaks of the FLC were easily found, even using unfractionated crude samples. Immobilization of the FLC onto gold-coated chips, and their subsequent SPR analyses were successively accomplished, as had been performed previously using non-fluorescent ligand conjugates.

Key words: immobilization, sugar chain, high sensitivity, analysis, fluorescence, linker molecule, mass spectrometry.

Abbreviations: DMAc, N, N-dimethyl acetoamide; aoWS, N^{α}-((aminooxy)acetyl)tryptophanylarginine methyl ester.

The carbohydrates that make up proteoglycans, glycoproteins or glycolipids are responsible for many biological functions and play crucial roles in cellular binding and signalling (*1*). However, because of their structural complexity, the methods for studying sugar chains are more challenging than that for DNA, RNA or proteins. The numerous isomeric and anomeric configurations of sugar chains, as well as the difficulties in isolating sufficient quantities of naturally occurring sugars, make binding analysis and structure–function studies challenging.

For the structural analysis of naturally occurring sugar chains, fluorescent labelling of the sugars has been one popular technique (*2*). Recently, mass spectrometry (MS) has been used for structural analysis of sugar structures, thanks to the development of structurally well-defined standards (*3, 4*). Surface plasmon resonance (SPR) methodology is also a very effective method to quantify binding interactions between sugar-chains and lectins or viruses in real time, because it is a non-destructive technology that does not require large quantities of the often scarce materials to be studied (*5–9*). We have previously reported the development of the 'sugar chip', in which defined sugar chains are immobilized on an SPR sensor chip using our specialized linker molecules (*10, 11*). But the purification of these linker-carbohydrate conjugates for SPR has been difficult when the quantities of the target sugar chains were limited (*i.e.* <1 mg). To overcome this and the other challenges in the analysis of scarce sugar chains, we have developed a novel carbohydrate linker molecule that is also fluorescent (named 'f-mono'). Here we report the successful synthesis of this novel fluorescent linker molecule, and the preparation and purification of conjugates (fluorescent ligand-conjugate or FLC) using as little as 1 μg of sugar chain. These FLCs were then effectively employed in SPR analysis of carbohydrate–protein binding, as well as MS and MS/MS structural analyses.

MATERIALS AND METHODS

General Procedure—All reactions in organic media were carried out with freshly distilled solvents or with

*To whom correspondence should be addressed. Tel: +81-99-285-8369, Fax: +81-99-285-8369, E-mail: ysuda@eng.kagoshima-u.ac.jp

commercially available extra grade solvents purchased from Kanto Chem. Co. (Tokyo, Japan), Nacalai Tesque (Kyoto, Japan) or Wako Chem. Co. (Osaka, Japan). Silica gel column chromatography was performed using PSQ 60B (Fuji Silysia Chem. Ltd., Aichi, Japan). Electrospray ionization time-of-flight mass (ESI-TOF/MS) spectra were obtained by Mariner™ (Applied Biosystems, Framingham, MA, USA). ^{1}H-NMR measurements were performed with JEOL (Tokyo, Japan) ECA-600.

Synthesis of f-mono linker—2,6-Diaminopyridine (1.06 g, 9.70 mmol, Sigma, USA) and thioctic acid (1.00 g, 4.80 mmol, Sigma, USA) were dissolved in anhydrous *N, N*-dimethylformamide (10 ml). Then, 1-hydroxy-7-azabenzotriazole (HOAt, 0.66 g, 4.80 mmol), 1-ethyl-3-(3-dimethylaminopropyl)carbodiimide monohydrochloride (EDC-HCl, 0.93 g, 4.80 mmol), and diisopropylethylamine (DIEA, 0.84 ml, 4.80 mmol) were added to the solution. After stirring for 6 h under argon gas, the reaction product was extracted into the organic phase using dichloromethane (CH_2Cl_2, 20 ml), and was washed with water (10 ml) three times and then with saturated sodium bicarbonate aqueous solution. The product was then purified by silica gel column chromatography (80 g, eluted with toluene/ethyl acetate = 3/1, v/v) to obtain a yellow solid. Yield: 1.37 g (95%). MS calcd. for $C_{13}H_{19}N_3OS_2$: 297.10, Found: *m/z* 298.12 $[M+H]^+$; ^{1}H NMR (600 MHz, CDCl3), δ7.58 (1H, s), 7.53 (1H, d, J = 7.5 Hz), 7.46 (1H, t, J = 7.6, J = 8.2 Hz), 6.26 (1H, d, J = 8.2 Hz), 4.24 (1H, m), 3.59–3.56 (1H, m), 3.19–3.10 (2H, m), 2.48–2.44 (1H, m), 2.37–2.34 (2H, m), 1.93–1.90 (1H, m), 1.77–1.68 (4H, m), 1.53–1.48 (2H, m).

Preparation of a Conjugate with Lactose—Lactose monohydrate (20 mg, 56 μmol) and f-mono (18 mg, 61 μmol) were dissolved in a 2.2 ml solution of H_2O/AcOH/DMAc = 5/1/5 (v/v/v). After stirring for 5 h, sodium cyanoborohydrate (17 mg, 280 μmol) was added to the solution. The reaction mixture was left standing at 37°C for 1.5 days and lyophilized. The residue was dissolved in water and purified with an ODS column (20 g, 1.8 cmΦ × 46 cm, eluted with water/methanol = 1/1, v/v). The appropriate fraction was lyophilized with water to obtain the desired final product: fluorescent ligand-conjugate (FLC, abbreviated as Galβ1-4Glc-f-mono) as a white powder. Yield: 19 mg (50%). MS calcd. for $C_{25}H_{41}N_3O_{11}S_2$: 623.17, Found: m/z 624.17 $[M+H]^+$; ^{1}H NMR (600 MHz, MeOD), δ 7.31 (1H, d, J = 8.1 Hz), 6.99 (1H, d, J = 2.0 Hz), 6.20 (1H, d, J = 8.0 Hz), 4.28 (1H, d, H-1′), 3.89 (1H, dd, H-4), 3.75 (2H, m, H-2, H-5), 3.63 (3H, m, H-3, H-6a, H-6b), 3.52 (1H, m), 3.45 (1H, m, H-4′), 3.30 (2H, m, H-3′, H-5′), 3.25–3.14 (2H, m, H-1a,H-2′), 3.05–2.94 (3H, m, H-1b), 2.36 (1H, m), 2.26 (2H, t, J = 7.3 Hz), 1.84–1.76 (1H, m), 1.54–1.35 (6H, m).

Preparation of a Conjugate with Maltose—Maltose (20 mg, 56 μmol) and f-mono (18 mg, 61 μmol) were dissolved in a 2.2 ml solution of H_2O/AcOH/DMAc = 5/1/5 (v/v/v). After stirring for 5 h, sodium cyanoborohydrate (17 mg, 280 μmol) was added to the solution. The reaction mixture was left standing at 37°C for 1.5 days, and lyophilized. The residue was dissolved in water and purified with ODS column (20 g, 1.8 cmΦ × 46 cm, eluted with water/methanol = 1/1, v/v). The appropriate fraction was lyophilized with water to obtain Glcα1-4Glc-f-mono as a white powder. Yield: 17 mg (46%). MS calcd. for $C_{25}H_{41}N_3O_{11}S_2$: 623.17, Found: m/z 624.17 $[M+H]+$; ^{1}H NMR (600 MHz, MeOD), δ 7.32 (1H,d), 6.99 (1H, d), 6.20 (1H, d), 4.95 (1H, s, H-1′), 3.89–3.78 (3H, m, H-2, H-4, H-5), 3.63 (3H, m, H-3, H-6a, H-6b), 3.42 (1H, m), 3.38 (1H, d, H-4′), 3.13 (2H, m, H-3′, H-5′), 2.85–2.3 (5H, m, H-1a,H-2′), 3.05–2.94 (3H, m, H-1b), 2.36 (1H, m), 1.74–1.26 (7H, m).

SPR Analysis—SPR experiments were perfomed with a 12-channel SPR machine (Moritex Co., Yokohama, Japan) using the manufacturer's recommended guidelines with slight modification. Sensor chips used for SPR experiments were prepared as follows. The gold-coated chip was purchased from SUDx-Biotec (Kagoshima, Japan), and washed in ozone cleaner. The chip was soaked in a 10-, 1-, or 0.1-μM solution of Galβ1-4Glc-f-mono or Glcα1-4Glc-f-mono, dissolved in methanol/water = 1/1 (v/v) at room temperature for 2 h or overnight, followed by subsequent washing with a methanol/water (1/1, v/v) containing 0.05% Tween-20, phosphate-buffered saline (PBS) at pH 7.4 containing 0.05% Tween-20, and PBS (pH 7.4). All washings were done with ultra-sonication for 20 min.

Binding studies were performed between test proteins in the aqueous phase and the stated sugars immobilized via fluorescent linkers (f-mono) attached to the sugar chips. The test proteins concanavalin A (Con A, EY Laboratories, San Mateo, CA, USA), RCA120 (Ricinus Communis Agglutinin I, Vector Laboratories, Servion, Switzerland), and bovine serum albumin (BSA, Nakalai Tesque) were perfused in the aqueous phase (PBS with 0.05% Tween-20 at pH 7.4) at a flow rate of 15 μl/min at 25°C.

Fluorescent Spectra—Fluorescent spectra were measured with a Spectro Fluorometer FP-6310 (JASCO, Tokyo, Japan). The concentration of f-mono was 100 μg/ml in $CHCl_3$. For comparison, our previous mono-valent non-fluorescent linker molecule [abbreviated as 'mono' in this paper (*11*)] was dissolved in $CHCl_3$ at 100 μg/ml, and used as a control.

Mass Spectrometry—MS and MS/MS spectra of FLCs were obtained with an AXIMA-QIT (Shimadzu, Kyoto, Japan), which is a quadrupole ion trap and matrix-assisted laser desorption/ionization time-of-flight mass spectrometer (QIT-MALDI-TOF/MS). Acquisition and data processing were controlled by the manufacturer's software (Kratos Analytical, Manchester, UK). For matrix, a purified 2,5-dihydroxybenzoic acid (DHBA) was dissolved in a mixed solvent with double distilled water containing 0.1% TFA/acetonitrile = 3/1 (v/v) at 10 mg/ml. To 1 μl of sample dissolved in the above mixed solvent spotted on a stainless-steel target, an equal volume of matrix solution was placed and allowed to dry.

Preparation of f-mono-Labelled Glycans from Human IgG—One hundred micrograms of human IgG (Institute of Immunology Co., LTD., Tokyo, Japan) was dissolved in 5 μl of H_2O and 5 μl of 1 M aqueous NH_4HCO_3, and 5 μl of 120 mM aqueous dithiothreitol were added. The reaction solution was heated at 60°C for 30 min. Then, 10 μl of 123 mM aqueous iodoacetamide was added. After incubation in the dark at room temperature for an hour, 10 μl of

trypsin (Sigma-Aldrich, 40 U/μl, dissolved in 1 mM HCl) was added. After an hour, trypsin was inactivated by heating at 90°C for 5 min. Then, 10 U of PNGase F (Roche, Switzerland) was added to the solution (*12*). After incubating at 37°C for 12 h, the solution was lyophilized.

The lyophilized residue was dissolved in 20 μl of H_2O, and concentrated by Blot Glyco (Kit No. MALDI type BS-45601S, Sumitomo Bakelite Co., Ltd. Tokyo, Japan) (*13*, *14*). At the final stage, using the manufacturer's guideline, N-glycans from IgG were released in H_2O, lyophilized and transformed to fluorescent ligand conjugates as follows. The mixture of naturally occurring lyophilized N-glycans and f-mono (100 mg, 340 μmol) were dissolved in 1.0 ml of a mixed solvent (H_2O/AcOH/DMAc = 5/1/5, v/v/v). After 5 h, sodium cyanoborohydrate (62 mg, 1.0 mmol) was added to the solution. The reaction mixture was left standing at 37°C for 1.5 days and lyophilized. To the residue, 200 μl of H_2O was added. Then, the aqueous phase was washed three times with 200 μl of phenol/$CHCl_3$ (1:1, v/v). The aqueous layer was concentrated in vacuo, and excess f-mono and other chemical reagents were removed using an ODS short column attached to the kit. For comparison, the N-glycans of IgG were transformed to the 'sugar-aoWRs condensation product (*15*)' according to the manufacturer's manual. The labelled N-glycans were examined by HPLC (Pump: L-6200, HITACHI, Tokyo, Japan; Detector: FP 2020, JASCO, Tokyo, Japan; Column: COSMOSIL $5C_{18}$-PAQ Waters, Nacalai Tesque; Elution: H_2O/MeOH = 1/1, v/v), and by mass spectrometry as described above.

RESULTS AND DISCUSSION

Introducing fluorescence into the linker was accomplished by replacing the 2,6-diaminobenzene unit of our original linker molecule (mono) (*11*), with a 2,6-diaminopyridine moiety (Scheme 1). The labelling of sugar chains using 2-aminopyridine (PA) reported by Hase *et al.* (*16*) was a pioneering advance for the analysis of trace amounts of sugar-chains, and has been applied to 2- or 3-dimensional mapping by Takahashi *et al.* (*17*, *18*) for the conventional structural identification of sugar chains from natural sources, such as glycoproteins. The high fluorescence of the 2,6-diaminopyridine moiety has also been well established, and its use for the biotinylation or immobilization of sugar chains has been reported (*19*, *20*). As expected, our novel f-mono linker molecule showed fluorescence at an excitation (ex) maximum of 335 nm and an emission (em) maximum of 380 nm. Since the sensitivity of detection of fluorescence is about 1,000 times higher than that of UV/VIS, a small quantity (~1 nmol) of sugar chain can be effectively derivatized by using this f-mono linker molecule. In addition, the molecular absorption coefficient (ε value) of f-mono was five times higher than that of the original linker molecule from which it was derived, indicating increased sensitivity even with a standard UV/VIS detector.

Figure 1 shows the SPR data of Con A, RCA120 and BSA binding to α-glucose or β-galactose immobilized *via* FLCs prepared with the f-mono linker to the sensor chip. BSA was used as a negative control, because our previous investigation (*21*) showed that it does not bind to

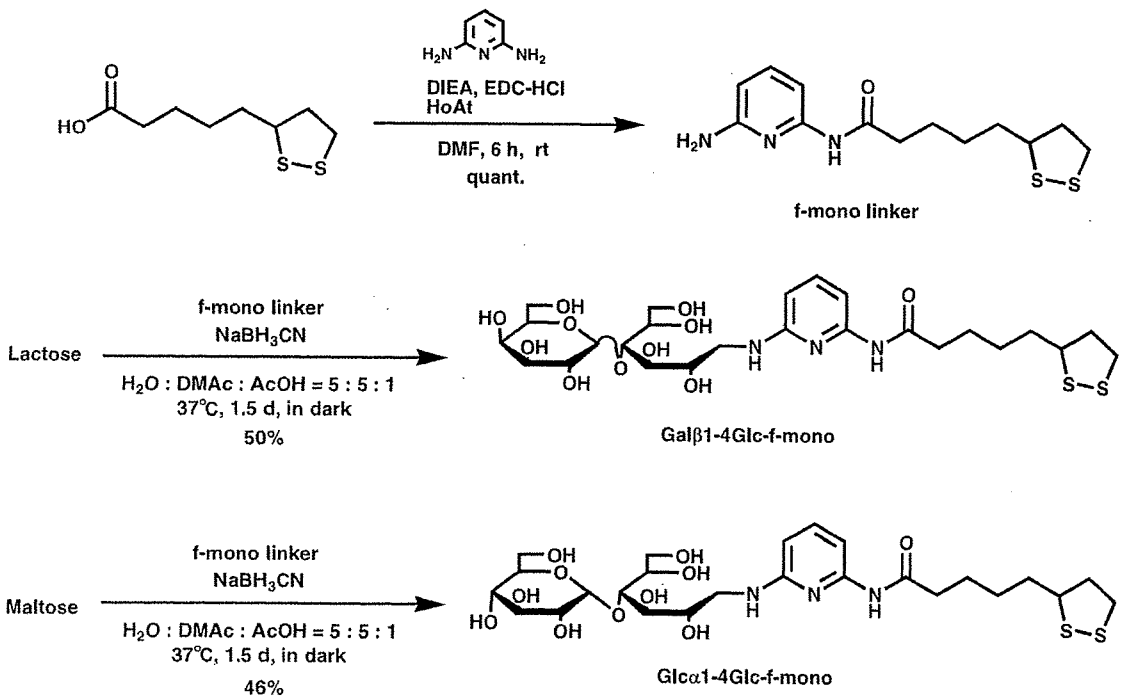

Scheme 1. **Synthesis of f-mono linker and preparation of ligand conjugates, Galβ1-4Glc-f-mono and Glcα1-4Glc-f-mono.**

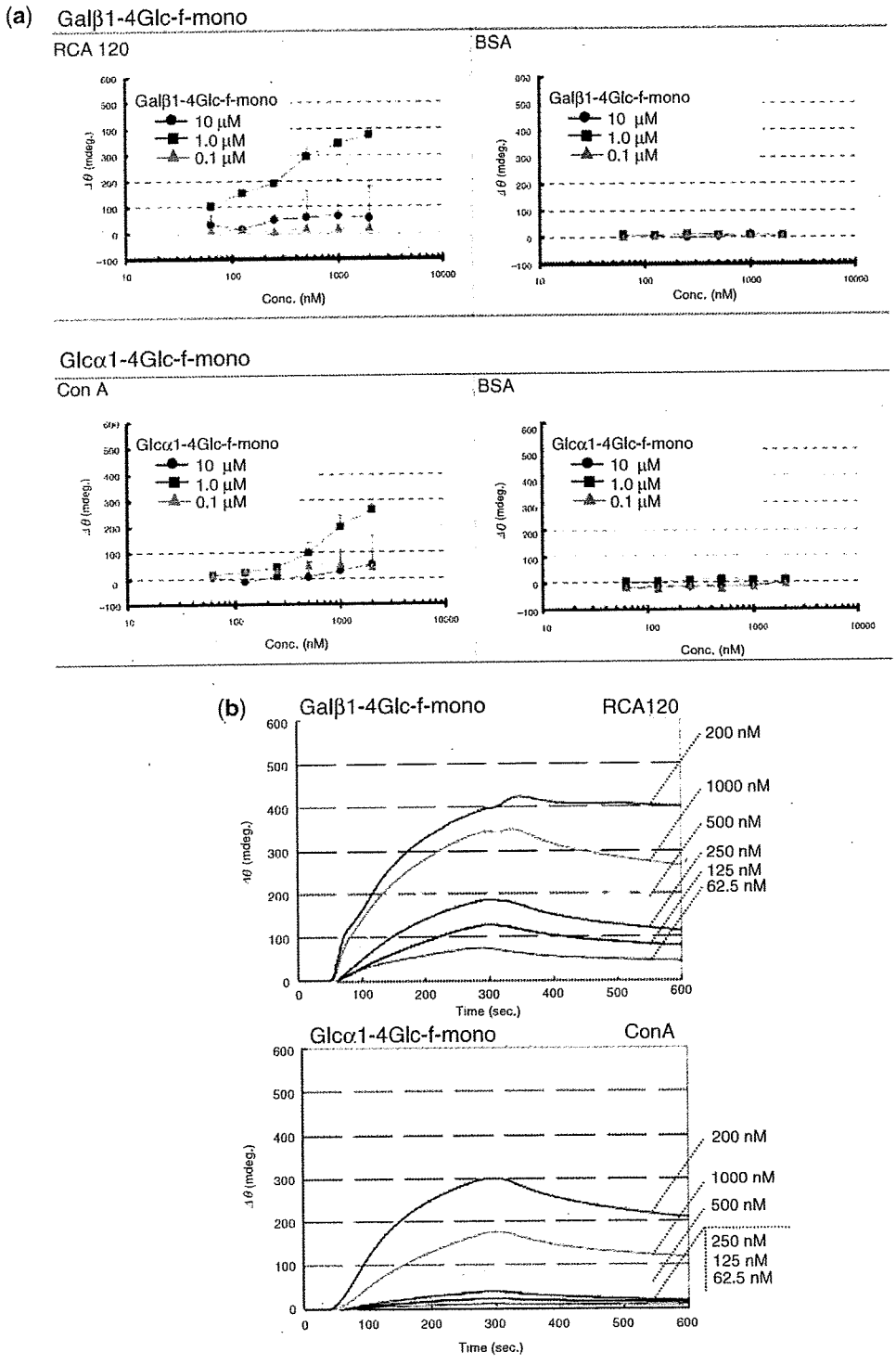

Fig. 1. **SPR analysis of lectins (Con A and RCA120) binding to defined sugars.** Galβ1-4Glc-f-mono or Glcα1-4Glc-f-mono were immobilized on gold-coated chips (see MATERIALS AND METHODS section for details). The test proteins were perfused in the aqueous phase (PBS with 0.05% Tween-20 at pH 7.4) at a flow rate of 15 μl/min at 25°C using a 12-channel SPR machine (Moritex Co., Tokyo, Japan). (a) Dependency of the lectin binding on concentration of FLCs immobilized on the chip. (b) SPR sensorgrams of RCA120 for the Galβ1-4Glc-f-mono chip, and Con A for the Glcα1-4Glc-f-mono chip, immobilized at 1 μM.

α-glucose or β-galactose. Figure 1(a) illustrates the dependency of protein binding on the density of immobilization of the sugar chain *via* FLCs on the chip. The data suggest that the optimal density for immobilization of both FLCs appears to be ~1 μM. At higher concentrations, steric hindrance due to the high concentration of ligands may occur and prevent the binding of protein. At 0.1 μM of FLC the ligand sugar chains may be too diluted on the chip to effectively bind protein, because of non-clustered ligands.

Using the chip immobilized with Galβ1-4Glc-f-mono, it was detected that RCA120 bound, but Con A and BSA did not. In contrast, using the chip with Glcα1-4Glc-fmono, Con A bound, but RCA120 and BSA did not. The binding of BSA to the sensor chips was negligible.

Figure 1(b) shows typical sensorgrams of RCA120 and Con A binding to the appropriate sugar chip. The calculated binding parameters were in agreement with those in the literatures (*22*, *23*) and with our previous data using a non-fluorescent linker molecule. The kinetic parameters were; RCA120 *vs.* Galβ1-4Glc-f-mono, $k_{on} = 6.3 \times 10^3\,M^{-1}s^{-1}$, $k_{off} = 4.1 \times 10^{-3}\,s^{-1}$, $K_D = 0.66\,\mu M$; Con A *vs.* Glcα1-4Glc-f-mono, $k_{on} = 2.5 \times 10^3\,M^{-1}s^{-1}$, $k_{off} = 3.1 \times 10^{3}\,s^{-1}$, $K_D = 1.2\,\mu M$.

The results of MS and MS/MS analyses of Galβ1-4Glc-f-mono are shown in Fig. 2. A set of two unique peaks was detected. In addition to the regular $[M+H]^+$ and

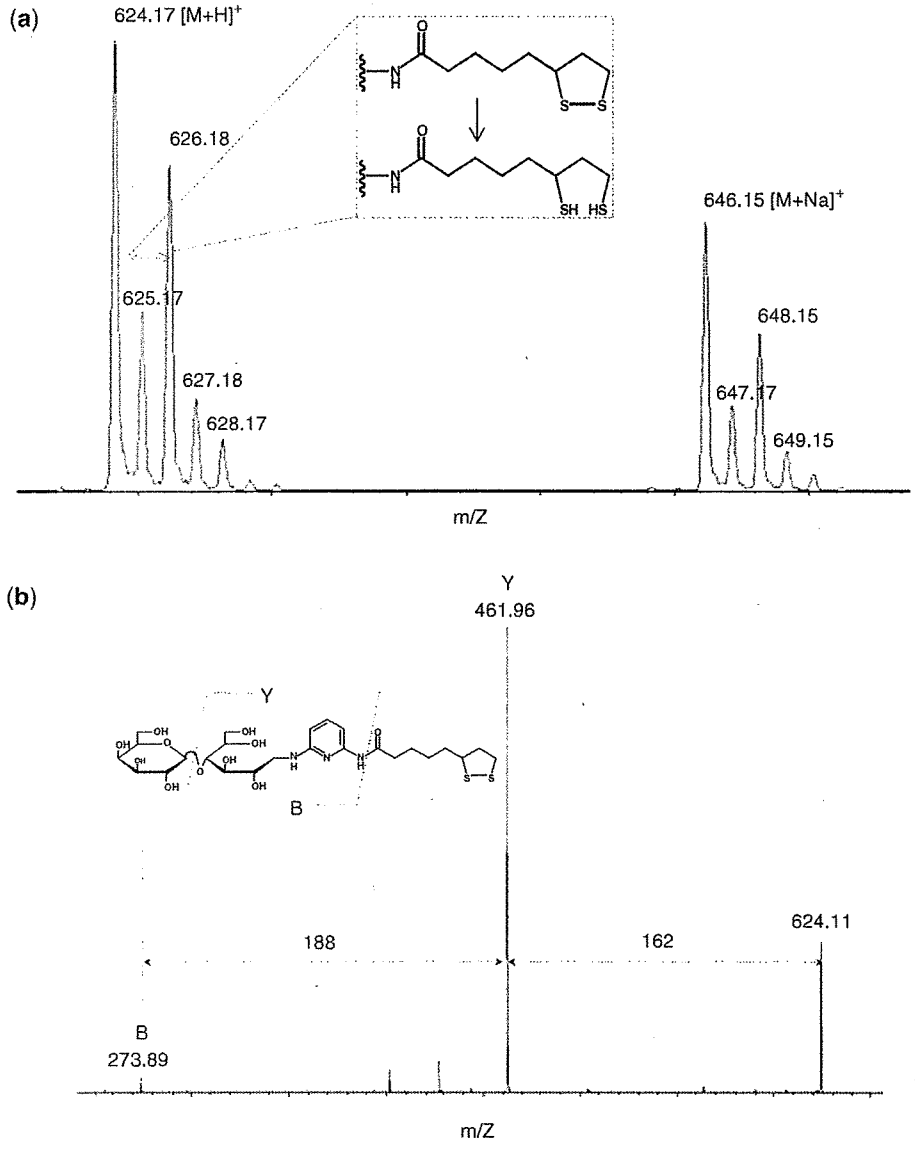

Fig. 2. **MS and MS/MS analyses of Galβ1-4Glc-f-mono.** A quadrupole ion trap and matrix-assisted laser desorption/ionization time-of-flight mass spectrometer (AXIMA-QIT) was used (see MATERIALS AND METHODS section for details). (a) MS spectrum of Galβ1-4Glc-f-mono; (b) MS/MS analysis of Galβ1-4Glc-f-mono.

$[M+Na]^+$ ion, 2-Da bigger peaks ($[M+H+2]^+$ and $[M+Na+2]^+$) were found [Fig. 2(a)]. These later peaks were derived from the reduction of the disulphide bond in the thioctic acid moiety of f-mono, since DHB (the matrix for MALDI) tends to reduce samples with the laser energy (*24*). This property of the f-mono linker was very useful for distinguishing MS peaks of f-mono-labelled glycans from contaminating peaks. In the MS/MS analysis, peaks lacking a galactose unit and thioctic acid from the precursor ion (m/z 624) were observed [Fig. 2(b)]. The cleavage here was as simple in the MS/MS analysis as that using PA-labelled sugar chains (*3*), facilitating structural analysis. For analysing structure and identifying specific sugars, the f-mono linker greatly enhanced the ability to recognize the labelled glycans. From these results, it is suggested that our f-mono linker is a highly effective reagent for MS analysis, at least in a system employing MALDI-QIT and DHBA.

Next, the N-glycans of human IgG were analysed using f-mono. As described in MATERIALS AND METHODS section, N-glycans were extracted from human IgG, concentrated, and then reacted with f-mono. Figure 3 shows the HPLC profile. Two fractions were collected and analysed using MS and MS/MS to confirm f-mono-labelled N-glycans (Fig. S1). From the MS and MS/MS, 162 or 203 different peaks were obtained, suggesting the carbohydrate-derived compounds. In addition, the f-mono labelled glycans were quite easily visualized as +2-Da differentially larger peaks in MS. From the calibration curve (Fig. S2) prepared with Galβ1-4Glc-f-mono, 518 pmol of labelled compounds were estimated to obtain from 100 μg of IgG using the HPLC results, and the detection limit in our HPLC system was estimated to be 5 pmol in 10 μl of injected sample solution.

For comparison, the released N-glycans were also labelled with a reagent (aoWRs) from the kit for MS.

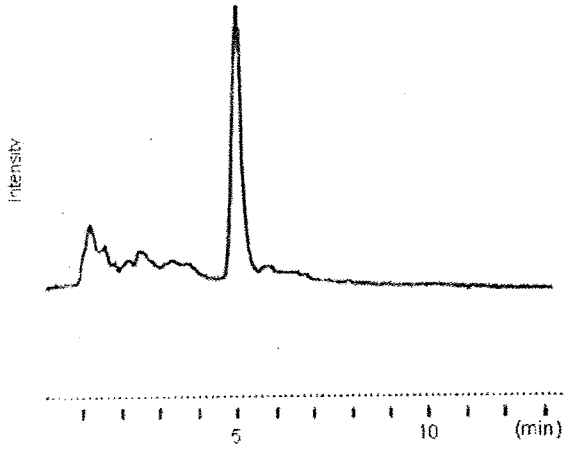

Fig. 3. **HPLC profile of f-mono labelled N-linked sugar chains from IgG.** The extraction of N-glycan and its labelling are described in the MATERIALS AND METHODS section. The conditions of HPLC were as follows. Column: COSMOSIL $5C_{18}$-PAQ Waters (Nacalai Tesque, 4.6 × 150 mm); elution: methanol/water = 1/1 (v/v).

By HPLC analysis, aoWRs-labelled N-glycans did not reveal any detectable peaks because aoWRs had no fluorescence. The MS data are summarized in Fig. 4. The MS spectrum of aoWRs-labelled N-glycans showed six glycan peaks clearly [Fig. 4(a)]. But in the case of the f-mono-labelled glycans, four additional glycans were clearly detected in the MS spectrum [Fig. 4(b)]. Furthermore, the larger 2-Da ions were observed as described above. Figure 4(c) shows the MS/MS spectrum of m/z 1947.1 ions of f-mono-labelled N-glycans. A wealth of structural information could be obtained from this spectrum. For example, from this peak the structure of the glycan containing four hexosamines and five hexoses was easily disclosed. In contrast, the MS/MS analysis of aoWRs-labelled glycan was not possible (data not shown).

The fluorescent intensity of the f-mono reagent was about 1/3 compared to that of 6-aminopyridine (PA) at the same concentration. Therefore, as judged by fluorescent intensity alone, the f-mono reagent is less sensitive. PA-derivatized sugar chains can be analysed by MS, but the f-mono derivatized one can be more easily detected because +2 Da differentially larger peaks are seen every time. Therefore, the novelty of this f-mono reagent is not the improvement of fluorescent sensitivity, but the significant improvement in MS peak identification. Moreover, the derivatized and analysed sugar chain with f-mono can be immobilized on SPR sensor chip sequentially. That is, the extensive merit of this f-mono reagent is that a more-comprehensive and integrated analysis of sugar chains can be sequentially performed using HPLC, MS and SPR.

The difficulty of synthesizing rigorously, structurally defined sugar chains remains a significant challenge to structure–function studies of carbohydrates. Narimatsu and colleagues (*25*) have made important advances in the preparation of sugar-chains using glycosyltransferases, and this synthetic approach holds promise. However, at this time, it is still challenging to prepare large, complex sugar chains. Therefore, for structure–function analyses, approaches that are economical in their use of scarce sugar chains have advantages. One solution is the SPR sugar-chip approach we have illustrated here. By immobilizing the sugar chains on the chip one can use it multiple times. In this case, it is a key to have an efficient linker molecule for immobilization of trace amounts of the defined sugar chain, of which the f-mono linker molecule is a good example.

In conclusion, the f-mono linker molecule is easily synthesized and its ligand-conjugates are easily purified. The labelled glycans are able to be traced with HPLC because of their fluorescence, making this a good application for trace amounts of glycan (~1 pmol/μl). Furthermore, the labelled glycan can be used for binding experiments using SPR, as we have previously demonstrated with non-fluorescent linker-conjugates. MS and MS/MS analyses of f-mono-labelled glycan were possible and effective in determining the glycan's primary structure, because the larger 2-Da ion peaks could be used to distinguish the labelled glycan-derived peaks. With this novel linker molecule, both the structural and functional binding analysis of trace amount of glycans are greatly facilitated, suggesting that this fluorescent linker

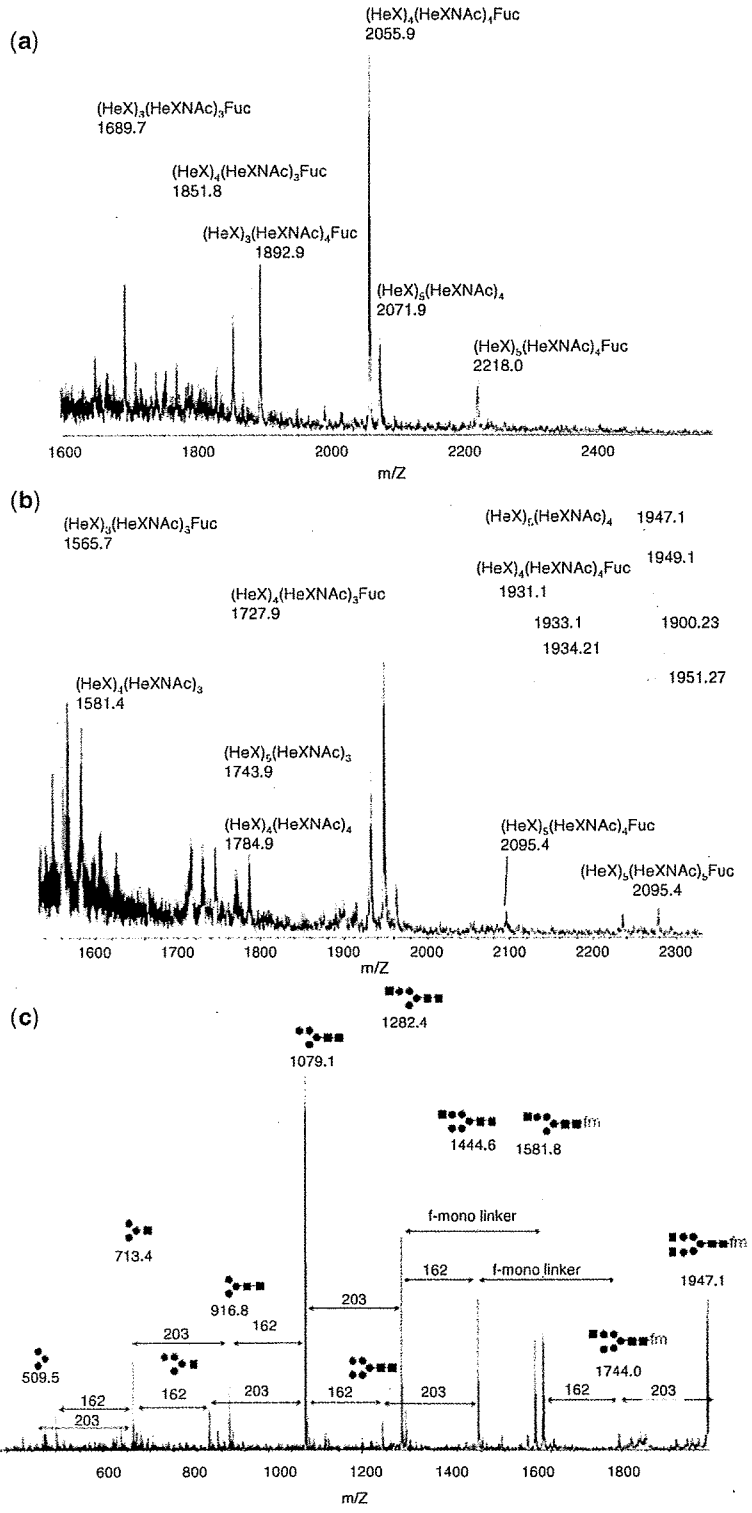

Fig. 4. **MS and MS/MS analyses of labelled N-linked sugar chains from IgG.** From 100 μg of human IgG, N-linked sugar chains were liberated by PNGase F, and concentrated by Blot Glyco (Sumitomo Bakelite Co., Ltd. Tokyo, Japan). The N-glycans were then released in H_2O, lyophilized and transformed to f-mono labelled or aoWRs conjugates as described in MATERIALS AND METHODS section. The labelled N-glycans were examined with mass spectrometry as described above. (a) aoWRs-labelled N-glycans. (b) f-mono labelled N-glycans. (c) MS/MS analysis of a peak ($m/z = 1497.1$) from the MS of f-mono labelled N-linked sugar chain from IgG.

technology should be a useful tool in the study of proteoglycomics.

SUPPLEMENTARY DATA

Supplementary data are available at *JB* online.

FUNDING

The Frontier Science Research Center (FSRC) of Kagoshima University (to Y.S.); Japan Science and Technology Agency (to Y.S.); Japanese Hyogo Prefecture (to Y.S.); and the National Institutes of Health, NHLBI (HL079182 to M.S.).

CONFLICT OF INTEREST

Nature of conflict of interest: Financial

Name of the author with conflict of interest: Y.S.

Entity and nature of the holdings: SUDx-Biotec Corporation

Amount of the holdings: 160/810 (19.753%)

Nature of conflict of interest: Management/Advisory Affiliations

Name of the author with conflict of interest: Y.S.

Nature of the relationships and financial arrangements: President and CSO of SUDx-Biotec Corporation. No financial arrangement.

Nature of conflict of interest: Patent

Name of the author with conflict of interest: M.S., Y.I., N.A., M.B., M.W. and Y.S.

Details and status: Japan Patent Submission #2008-108561 [Pending].

REFERENCES

1. Varki, A. (1999) In *Essentials of Glycobiology* (Varki, A., Cummings, R., Esko, J., Freeze, H., Hart, G., and Marth, J., eds.), *Cold Spring Horbor Laboratory Press*, Cold Spring Harbor, New York, pp 57–68 and references there in.
2. Kalyan, R.A. (2006) Advance in fluorescence derivatization methods for high-performance liquid chromatographic analysis of glycoprotein carbohydrates. *Anal. Biochem.* **350**, 1–23
3. Ojima, N., Masuda, K., Tanaka, K., and Nishimura, O. (2005) Analysis of neutral oligosaccharide for structural characterization by matrix-assisted laser desorption/ionization quadrupole ion trap time-of-flight mass spectrometry. *J. Mass Spectrom.* **40**, 380–388
4. Kameyama, A., Nakayama, S., Ito, H., Kikuchi, N., Angata, T., Nakamura, M., Ishida, H., and Narimatsu, H. (2006) Strategy for simulation of CID spectra of N-linked oligosaccharides toward glycomics. *J. Proteome Res.* **5**, 808–814
5. Plant, A.L., Brigham-Burke, M., Petrella, E.C., and O'Shannessy, D.J. (1995) Phospholipid/alkanethiol bilayers for cell-surface receptor studies by surface plasmon resonance. *Anal. Biochem.* **226**, 342–348
6. Petrlinz, K.A. and Georgiadis, R. (1996) In situ kinetics of self-assembly by surface plasmon resonance spectroscopy. *Langmuir* **12**, 4731–4740
7. Liedberg, B., Nylander, C., and Lundstrom, I. (1983) Surface plasmon resonance for gas detection and biosensing. *Sens. Actuators* **4**, 299–304
8. Flanagan, M.T. and Pantell, R.H. (1984) Surface plasmon resonance and immunosensors. *Electron. Lett.* **20**, 968–970
9. Matsubara, K., Kawata, S., and Minami, S. (1988) Optical chemical sensor based on surface plasmon measurement. *Appl. Opt.* **27**, 1160–1163
10. Suda, Y., Kusumoto, S., Arano, A., and Sobel M., US Patent 7,320,867 (2008. 1.22).
11. Suda, Y., Arano, A., Fukui, Y., Koshida, S., Wakao, M., Nishimura, T., Kusumoto, S., and Michael, S. (2006) Immobilization and clustering of structurally defined oligosaccharides for sugar chips: an improved method for surface plasmon resonance analysis of protein-carbohydrate interactions. *Bioconj. Chem.* **17**, 1125–1135
12. Kita, Y., Miura, Y., Furukawa, J., Nakano, M., Shinohara, Y., Ohno, M., Takimoto, A., and Nishimura, S.-I. (2007) Quantitative glycomics of human whole serum glycoproteins based on the standardized protocol for liberating N-glycans. *Mol. Cell Proteom* **6**, 1437–1445
13. Shimaoka, H., Kuramoto, H., Furukawa, J., Miura, Y., Kurogochi, M., Kita, Y., Hinou, H., Shinohara, Y., and Nishimura, S.-I. (2007) One-pot solid-phase glycoblotting and probing by transoximization for high-throughput glycomics and glycoproteomics. *Chem. Eur. J.* **13**, 4797–4804
14. Nishimura, S.-I., Niikura, K., Kurogochi, M., Matsushita, T., Fumoto, M., Hinou, H., Kamitani, R., Nakagawa, H., Deguchi, K., Miura, N., Monde, K., and Kondo, H. (2005) High-throughput glycomics: combined use of chemoselective glycoblotting and MALDI-TOF/TOF Mass spectrometry. *Angew. Chem. Int. Ed.* **44**, 91–96
15. Shinohara, Y., Furukawa, J., Niikura, K., Miura, N., and Nishimura, S.-I. (2004) Direct N-glycan profiling in the presence of tryptic peptides on MALDI TOF by controlled ion enhancement and suppression upon glycan-selective derivatization. *Anal. Chem.* **76**, 6989–6997
16. Hase, S., Ikenaka, T., and Matsushima, Y. (1978) Structure analysis of oligosaccharide by tagging of the reducing end sugars with a fluorescent compounds. *Biochem. Biophys. Res. Comm.* **85**, 257–263
17. Tomiya, N., Kurono, M., Ishihara, H., Tejima, S., Endo, S., Arata, Y., and Takahashi, N. (1987) Structural analysis of N-linked oligosaccharide by a combination of glycopeptidase, exoglycosidase, and high-performance liquid chromatography. *Anal. Biochem.* **163**, 489–499
18. Nakagawa, H., Kawamura, Y., Kato, K., Shimada, I., Arata, Y., and Takahashi, N. (1995) Identification of neutral and sialyl N-linked oligosaccharide structures from human serum glycoproteins using three kinds of high-performance liquid chromatography. *Anal. Biochem.* **226**, 130–138
19. Xuezheng, S., Baoyun, Xia, Yi, L., David, F.S., and Richard, D.C. (2008) Quantifiable fluorescent glycan microarrays. *Glycoconj. J.* **25**, 15–25
20. Munoz, J.F., Rumbero, A., Sinisterra, V.J., Santos, I.J., Andre, S., Gabius, H.J., Jimenez-Barbero, J., and Hernaiz, J.M. (2008) Versatile strategy for the synthesis of biotin-labelled glycans, their immobilization to establish a bioactive surface and interaction studies with a lectin on a biochip. *Glycoconj. J.* **25**, 633–646
21. Suda, Y., Kishimoto, Y., Nishimura, T., Yamashita, S., Hamamatsu, M., Saito, A., Sato, M., and Wakao, M. (2006) Sugar-immobilized gold nano-particles (SGNP): novel bioprobe for the on-site analysis of the oligosaccharide-protein interactions. *Polym. Preprints* **47**, 156–157
22. Heimholz, H., Cartellieri, S., He, L., Thiesen, P., and Niemeyer, B. (2003) Process development in affinity separation of glycoconjugates with lectins as ligands. *J. Chromatogr. A* **1006**, 127–135
23. Itakura, Y., Nakamura-Tsuruta, S., Kominami, J., Sharon, N., Kasai, K., and Hirabayashi, J. (2007) Systematic comparison of oligosaccharide specificity of Ricinus communis agglutinin I and Eryrina lectins: a search by frontal affinity chromatography. *J. Biochem.* **142**, 459–469

24. Sekiya, S., Yamaguchi, Y., Kato, K., and Tanaka, K. (2005) Mechanistic elucidation of formation of reduced 2-aminopyridine-derivatized oligosaccharide and their application in matrix assisted desorption/ionization mass spectrometry. *Rapid Commun. Mass Spectrom.* **19**, 3607–3611

25. Shirato, H., Ogawa, S., Ito, H., Sato, T., Kameyama, A., Narimatsu, H., Zheng, X., Miyamura, T., Wakita, T., Ishii, K., and Takeda, N. (2008) Noroviruses distinguish between Type 1 and Type 2 histo-blood group antigens for binding. *J. Virol.* **82**, 10756–10767

OPEN ACCESS Freely available online

PLoS one

The 3′-Phosphoadenosine 5′-Phosphosulfate Transporters, PAPST1 and 2, Contribute to the Maintenance and Differentiation of Mouse Embryonic Stem Cells

Norihiko Sasaki[1], Takuya Hirano[1], Tomomi Ichimiya[1], Masahiro Wakao[2], Kazumi Hirano[1], Akiko Kinoshita-Toyoda[3,4], Hidenao Toyoda[3,4], Yasuo Suda[2,4], Shoko Nishihara[1,4]*

1 Laboratory of Cell Biology, Department of Bioinformatics, Faculty of Engineering, Soka University, Hachioji, Tokyo, Japan, 2 Department of Nanostructure and Advanced Materials, Graduate School of Science and Engineering, Kagoshima University, Kohrimoto, Kagoshima, Japan, 3 Laboratory of Bio-analytical Chemistry, College of Pharmaceutical Sciences, Ritsumeikan University, Kusatsu, Shiga, Japan, 4 Core Research for Evolutional Science and Technology (CREST) of Japan Science and Technology Agency (JST), Kawaguchi, Saitama, Japan

Abstract

Recently, we have identified two 3′-phosphoadenosine 5′-phosphosulfate (PAPS) transporters (PAPST1 and PAPST2), which contribute to PAPS transport into the Golgi, in both human and *Drosophila*. Mutation and RNA interference (RNAi) of the *Drosophila PAPST* have shown the importance of PAPST-dependent sulfation of carbohydrates and proteins during development. However, the functional roles of PAPST in mammals are largely unknown. Here, we investigated whether PAPST-dependent sulfation is involved in regulating signaling pathways required for the maintenance of mouse embryonic stem cells (mESCs), differentiation into the three germ layers, and neurogenesis. By using a yeast expression system, mouse PAPST1 and PAPST2 proteins were shown to have PAPS transport activity with an apparent K_m value of 1.54 μM or 1.49 μM, respectively. RNAi-mediated knockdown of each *PAPST* induced the reduction of chondroitin sulfate (CS) chain sulfation as well as heparan sulfate (HS) chain sulfation, and inhibited mESC self-renewal due to defects in several signaling pathways. However, we suggest that these effects were due to reduced HS, not CS, chain sulfation, because knockdown of mouse *N-deacetylase/N-sulfotransferase*, which catalyzes the first step of HS sulfation, in mESCs gave similar results to those observed in *PAPST*-knockdown mESCs, but depletion of CS chains did not. On the other hand, during embryoid body formation, *PAPST*-knockdown mESCs exhibited abnormal differentiation, in particular neurogenesis was promoted, presumably due to the observed defects in BMP, FGF and Wnt signaling. The latter were reduced as a result of the reduction in both HS and CS chain sulfation. We propose that PAPST-dependent sulfation of HS or CS chains, which is regulated developmentally, regulates the extrinsic signaling required for the maintenance and normal differentiation of mESCs.

Citation: Sasaki N, Hirano T, Ichimiya T, Wakao M, Hirano K, et al. (2009) The 3′-Phosphoadenosine 5′-Phosphosulfate Transporters, PAPST1 and 2, Contribute to the Maintenance and Differentiation of Mouse Embryonic Stem Cells. PLoS ONE 4(12): e8262. doi:10.1371/journal.pone.0008262

Editor: Jose Alberola-Ila, Oklahoma Medical Research Foundation, United States of America

Received June 2, 2009; **Accepted** November 10, 2009; **Published** December 11, 2009

Funding: This research was partially supported by funds from Ministry of Education, Culture, Sports, Science and Technology (MEXT), the Grant-in-Aid for Scientific Research (B) to SN, 20370051, 2008–2010, and from MEXT, the Matching Fund for Private Universities, S0901015, 2009–2014. The funders had no role in study design, data collection and analysis, decision to publish, or preparation of the manuscript.

Competing Interests: The authors have declared that no competing interests exist.

* E-mail: shoko@t.soka.ac.jp

Introduction

Embryonic stem cells (ESCs) [1,2] are promising tools for biotechnology and possess key features that should allow their exploitation in the development of cell replacement therapies [3]. To exploit the potential of ESCs for therapeutic purposes, a better understanding of the molecular mechanisms that control the pluripotency and differentiation of ESCs is required. The factors that control the pluripotency of mouse ESCs (mESCs) are increasingly being defined and the regulation of pluripotency requires a combination of extrinsic and intrinsic factors [4,5]. A number of the intrinsic factors, such as Oct3/4 and Nanog, have been identified [6]. Recent studies have shown that mESCs and human ESCs (hESCs) maintain their pluripotency using different extrinsic factors.

Leukemia inhibitory factor (LIF) [7,8], which is one of the known extrinsic factors, plays an important role in maintaining the self-renewal of mESCs via the activation of STAT3 [9–12] and induction of c-Myc [13]. One of the other extrinsic factors involved in the maintenance of mESC self-renewal is bone morphogenic protein 4 (BMP4). BMP4 acts in synergy with LIF to maintain self-renewal via the Smad-mediated induction of *Id* (*inhibitor of differentiation*) gene expression [14] and inhibition of p38 mitogen-activated protein kinase [15]. Wnt/β-catenin signaling also plays a role in the regulation of self-renewal of both mESCs and hESCs and this signaling is independent of LIF/STAT3 signaling [16–19]. It has been demonstrated that signaling by the canonical Wnt pathway increases and maintains Nanog expression [16–18]. Thus, the activation of Nanog by Wnt/β-catenin signaling can sustain ESC self-renewal without the use of feeder cells or treatment with LIF [16,17].

To enable the production of differentiated cells of a specific lineage, the mechanism of regulation of extrinsic signaling in ESCs

has been investigated by applying knowledge obtained from analysis of the early mouse embryo. It is known that several extrinsic factors, such as BMP, fibroblast growth factor (FGF) and Wnt, play important roles in the differentiation of mESCs, in addition to their involvement in self-renewal [20]. BMP/Smad signaling is essential for the decision between ectodermal and mesodermal fates. It has been demonstrated that antagonism of BMP/Smad signaling, for example by exposure of mESCs to Noggin or by transfection with a Noggin-encoding plasmid, promotes neurectodermal differentiation via embryoid body (EB) formation [21,22]. FGF4 is produced in an autocrine fashion in mESCs and FGF4/extracellular signal-regulated kinase (ERK) signaling contributes to differentiation into neural and mesodermal lineages [23]. Wnt/β-catenin signaling inhibits neural differentiation via EB formation: either inactivation of the adenomatous polyposis coli (APC) protein, which regulates the activity of β-catenin, or the introduction of a dominant active form of β-catenin results in the inhibition of neural differentiation in mESCs [24]. Furthermore, the Wnt antagonist *Sfrp2* is expressed during the neural differentiation of EBs and expression of *Sfrp2* enhances neuronal differentiation [25].

Sulfation is an essential modification of many carbohydrates and proteins, and is necessary for normal growth and development. In higher organisms, all sulfation reactions require the high energy sulfate donor 3′-phosphoadenosine 5′-phosphosulfate (PAPS) [26]. PAPS is synthesized in the cytosol and nucleus by PAPS synthetase [27,28] and is subsequently translocated into the Golgi via the PAPS transporter (PAPST) [29–32] to serve as a substrate for sulfotransferases. Recently, we identified and characterized two homologues of PAPST (PAPST1 and PAPST2) in both human and *Drosophila* [29,31,32].

Mutations in the *Drosophila PAPST1* gene, *slalom*, are associated with defects in multiple signaling pathways, including Wnt/Wingless (Wg) and Hedgehog (Hh) signaling, and in the determination of the embryonic dorsal/ventral axis [30]. These defects are suggested to be due to a lack of sulfation of heparan sulfate (HS) chains. HS, a sulfated glycosaminoglycan (GAG), is present ubiquitously as a cell surface proteoglycan. HS chains are known to play crucial roles in the regulation of several signaling pathways by controlling the binding of various extracellular signaling molecules, such as members of the FGF family, Wnt/Wg, Hh and BMP, to their cognate receptors [33]. Recently, we have also suggested that the second *Drosophila* PAPST, dPAPST2, contributes to signaling by Hh and Decapentaplegic by controlling HS chain sulfation [32]. It has been reported that mutants of the zebrafish *PAPST1* gene, *pinscher*, have cartilage defects that are analogous to those found in the zebrafish *dackel* mutant, which is HS chain defective [34]. The above genetic experiments have established that sulfation of GAGs is essential for normal development and that the regulation of sulfation is extremely important.

In mammals, the importance of HS chains during development has been demonstrated by the analysis of mutations in enzymes required for HS chain modification [33,35–38]. Recently, we have demonstrated that HS chains contribute to the self-renewal and pluripotency of mESCs and that this role involves the regulation of Wnt/β-catenin signaling [17]. Other groups have reported that HS chains contribute to the differentiation of mESCs into mesodermal and neurectodermal lineages [39,40]. Thus, there is evidence that HS chains have essential functions in development including in ESCs. However, the significance during development of the PAPST-dependent sulfation of either HS or other sulfated carbohydrates, such as chondroitin sulfate (CS), which is another major sulfated GAG and is implicated in the signaling pathway of heparin-binding growth factors [41,42], is not understood well.

In the present study, we analyzed the function of *PAPST1* and *PAPST2* by performing RNA interference (RNAi). Although the knockdown (KD) efficiency was less than 100%, we used this method rather than performing gene knockouts because, in addition to the direct effects of gene knockouts, secondary effects may also be observed that are caused by adaptation of the cells during long-term culture. For example, the expression of a novel gene might be induced that has secondary effects on the mESCs. If, as in the case of the *PAPST* genes, the RNAi targets are essential for cell survival and proliferation, analysis of the knockout cells may be complicated by cell death. In fact, knockout of some genes that are related to HS sulfation, e.g., *6-O-endosulfatase*, *C5-epimerase* and *HS2ST*, leads to a number of unexpected changes in the structure of sulfated GAGs, presumably due to secondary effects [36,38,43].

Our current understanding is that sulfated carbohydrates contribute to the maintenance and differentiation of ESCs by regulating the binding of extrinsic factors and subsequent signal transduction. In this study, we investigated the contribution of PAPST-dependent sulfation to the regulation of mESC self-renewal and pluripotency, differentiation into the three germ layers, and neurogenesis. First, we confirmed that the mouse solute carrier family 35B2 (SLC35B2) and SLC35B3 proteins, namely mouse PAPST1 and PAPST2, both exhibited PAPS transport activity. Then we showed that knockdown of either *PAPST1* or *PAPST2* in mESCs reduced the self-renewal and proliferation of the cells even in the presence of LIF and serum. These effects are likely to be due to the reduction of HS chain sulfation, because knockdown of mouse *N-deacetylase/N-sulfotransferase* (*NDST*), which encodes the enzyme responsible for the first step of HS sulfation, in mESCs resulted in similar effects but depletion of CS chains did not. Both *PAPST1*- and *PAPST2*-KD mESCs exhibited abnormal differentiation during EB formation. In particular, neurogenesis was promoted due to the reduction of both HS and CS chain sulfation. We highlight here the importance of PAPST-dependent sulfation for the maintenance of the self-renewal and pluripotency of mESCs and also the normal differentiation of EBs.

Results

Both Mouse *PAPST1* and *PAPST2* Are PAPS Transporter Genes

The human *PAPST1* and *PAPST2* genes are members of SLC35B. The mouse proteins SLC35B2 and SLC35B3 (NCBI accession numbers NP_082938 and NP_598821, respectively) share 82.41% and 83.54% homology with the human orthologs PAPST1 and PAPST2, respectively. Hydrophobicity analyses of the amino acid sequences using the SOSUI system (Mitsui Knowledge Industry Co., Ltd.) revealed that mouse PAPST1 and PAPST2 were type III transmembrane proteins with eight and nine transmembrane domains, respectively. The mouse *PAPST1* and *PAPST2* genes consist of four and ten exons, respectively, and both were expressed ubiquitously in all organs (Data not shown).

The substrate specificity of the mouse PAPST1 and PAPST2 proteins was examined using a yeast expression system in a manner similar to that used to investigate human PAPST1 and PAPST2 [29,31]. The coding sequence for hemagglutinin (HA)-tagged *PAPST1* or HA-tagged *PAPST2* was inserted into the yeast expression vector YEp352GAP-II. The constructs were then introduced into W303-1a yeast to allow preparation of the Golgi-enriched P100 membrane fraction that contained the mouse PAPST1 or PAPST2 protein. The HA-tagged PAPST1 and PAPST2 proteins were detected in the yeast P100 membrane

fraction by Western blotting using an antibody against the HA epitope tag (Figure 1A). The substrate specificity of the PAPST1 and PAPST2 proteins was examined using the P100 membrane fraction and radiolabeled substrates. The P100 membrane fractions prepared from yeast cells that expressed PAPST1 or PAPST2 showed PAPS transport activity that was significantly higher than that observed in the control cells (Figure 1B). The dependence of PAPS transport by PAPST1 and PAPST2 on substrate concentration is shown in Figure 1C. Both PAPST1 and PAPST2 showed a saturable PAPS transport activity with apparent K_m values that were estimated to be 1.54 μM and 1.49 μM, respectively.

Sulfation of Several Substrates Is Reduced by Knockdown of *PAPST* mRNA

To examine the effects of reduced sulfation in mESCs, we knocked down the expression of either *PAPST1* or *PAPST2* mRNA by RNAi. Real time PCR performed 2 days after transfection of the small interfering RNAs (siRNAs) showed that the level of *PAPST1* or *PAPST2* mRNA was reduced to approximately 40% of that in control cells (Figure 2A). The level of *PAPST1* mRNA was unaffected by the *PAPST2* siRNAs, and similarly the level of *PAPST2* mRNA was not decreased by the *PAPST1* siRNAs (Figure 2A), which confirmed the specificity of the targeting sequences. When the cells were transfected with both *PAPST1* and *PAPST2* siRNAs (*PAPST1+2*-KD cells), the level of both *PAPST1* and *PAPST2* mRNA was reduced to approximately 40% of that in control cells (Figure 2A). The results shown in this paper were obtained using the *PAPST1-1* and *PAPST2-1* siRNAs, however we obtained similar results using other siRNA sequences against *PAPST1* and *PAPST2* (Data not shown). For all experiments, we examined the effects of the knockdowns in the R1 mESC line first using two types of siRNA expression plasmid and then confirmed the effects in the E14TG2a line using a single siRNA expression plasmid.

We first examined endogenous PAPS transport activity in the mESCs. PAPS transport activities in both *PAPST1*- and *PAPST2*-KD cells were reduced to approximately 80% of that of control cells, which confirms that both the *PAPST1* and *PAPST2* genes encode a PAPST protein (Figure S1). We next determined by metabolic labeling whether total sulfate incorporation into cellular proteins in mESCs was reduced by knockdown of *PAPST1* or *PAPST2* mRNA. The radioactivity incorporated into cellular proteins in both *PAPST1*- and *PAPST2*-KD cells was approximately 80% of that incorporated in control cells (Figure 2B). Furthermore, sulfation of cell surface GAGs, such as HS and CS chains, in both *PAPST1*- and *PAPST2*-KD cells was significantly reduced to approximately 60–70% of that of control cells (Figure 2B). The *PAPST1+2*-KD cells showed the lowest incorporation value, indicating additive effect from reduction of both PAPST1 and PAPST2. In *PAPST1*-transfected MDCK II cells, chain length of GAGs was changed compared with non-transfected cells [44]. So, we examined length of HS and CS chains in both *PAPST1*- and *PAPST2*-KD cells, but no detectable differences between *PAPST*-KD cells and control cells were detected (Data not shown).

We performed FACS analysis to examine other sulfated substrates. Sulfatide SM3 (SO_3-3Galβ1-4Glcβ1-1Cer), one of the sulfated glycolipids, was reduced slightly in both *PAPST1*- and *PAPST2*-KD cells compared to that observed in control cells (Figure 2C). Other sulfated glycans and glycolipids, such as 3′-sulfo-Le^a (SO_3-3Galβ1-3(Fucα1-4)GlcNAc), human natural killer-1 (HNK-1) carbohydrate (SO_3-3GlcAβ1-3Galβ1-4GlcNAc) and sulfatide SM4 (SO_3-3Galβ1-1Cer), were not detected by FACS analysis (Data not shown), showing that such molecules were not present on the surface of mESCs.

These results demonstrate that both PAPSTs contribute comparably to the sulfation of proteins and several carbohydrates.

PAPST1- and PAPST2-Dependent Sulfation of HS Chains but Not CS Chains Is Important for the Self-Renewal and Proliferation of mESCs

We performed colony assays with *PAPST1*- and *PAPST2*-KD cells to determine whether reduced sulfation affected self-renewal. The number of colonies derived from either *PAPST1*- or *PAPST2*-KD cells that remained in an undifferentiated state fell to approximately 60% of the number from control cells even in the presence of LIF and serum in clonal density culture, showing reduction of self-renewal in *PAPST*-KD cells (Figure 3A). Furthermore, the most of the *PAPST1*- and *PAPST2*-KD cells exhibited a flattened, differentiated morphology in normal density culture four days after transfection (Figure S2A). These results are supported by the reduced expression of *Oct3/4* and *Nanog*, markers of the undifferentiated state, and up-regulated expression of extraembryonic endoderm (ExE) lineage markers, *Gata6* (primitive endoderm), *LamininB1* (parietal endoderm) and *Bmp2* (visceral endoderm) (Figure 3B and S2B). The above results demonstrate that both PAPST1- and PAPST2-dependent sulfation is important for the maintenance of the undifferentiated state and pluripotency of mESCs.

Next we examined proliferation. As shown in Figure 3C, the proliferation of both *PAPST1*- and *PAPST2*-KD cells decreased significantly compared to that of control cells. We have reported previously that HS chains contribute to the self-renewal and proliferation of mESCs [17], but the contribution of CS chains is unknown. Depletion of CS chains by treatment with chondroitinase ABC (ChABC) did not affect self-renewal and proliferation (Figure S3A and B), which demonstrated that CS chains do not contribute to these processes in mESCs. Furthermore, we examined whether a specific reduction in HS chain sulfation would result in similar defects to those observed in *PAPST*-KD cells. In mESCs, only *NDST1* and *NDST2* are expressed equally [45]. Therefore, we knocked down both *NDST1* and *NDST2* to avoid functional compensation. The effects of the knockdown were confirmed by RT-PCR analysis and metabolic labeling. In the *NDST1+2*-KD cells, the levels of both *NDST1* and *NDST2* mRNA were reduced to 39.5±4.9% and 34.0±2.8% of those in control cells, respectively, and sulfation of HS chains was reduced to 69.6±7.3% of that in control cells. As shown in Figure 3 and S2B, *NDST1+2*-KD cells exhibited similar defects in self-renewal and proliferation as the *PAPST*-KD cells. Thus, we conclude that the defects observed in *PAPST*-KD cells are due to a reduction in HS chain sulfation. In addition, the knockdown of both *PAPST1* and *PAPST2* together had an additive effect on self-renewal, and it is likely that the further reduction of HS sulfation observed in the *PAPST1+2*-KD cells, as shown in Figure 2B, was responsible for this additive effect.

Taken together, these results demonstrate that the reduction of PAPST1- and PAPST2-dependent sulfation inhibit both self-renewal and proliferation of mESCs, and this is presumably due to reduced levels of HS chain-dependent signaling.

The Reduction of PAPST-Dependent Sulfation Down-Regulates Several Signaling Pathways in mESCs

Several signaling molecules are important for the maintenance of mESC self-renewal and differentiation, e.g. LIF/STAT3, BMP/Smad, FGF/ERK and Wnt/β-catenin [9–12,14,16,17,23].

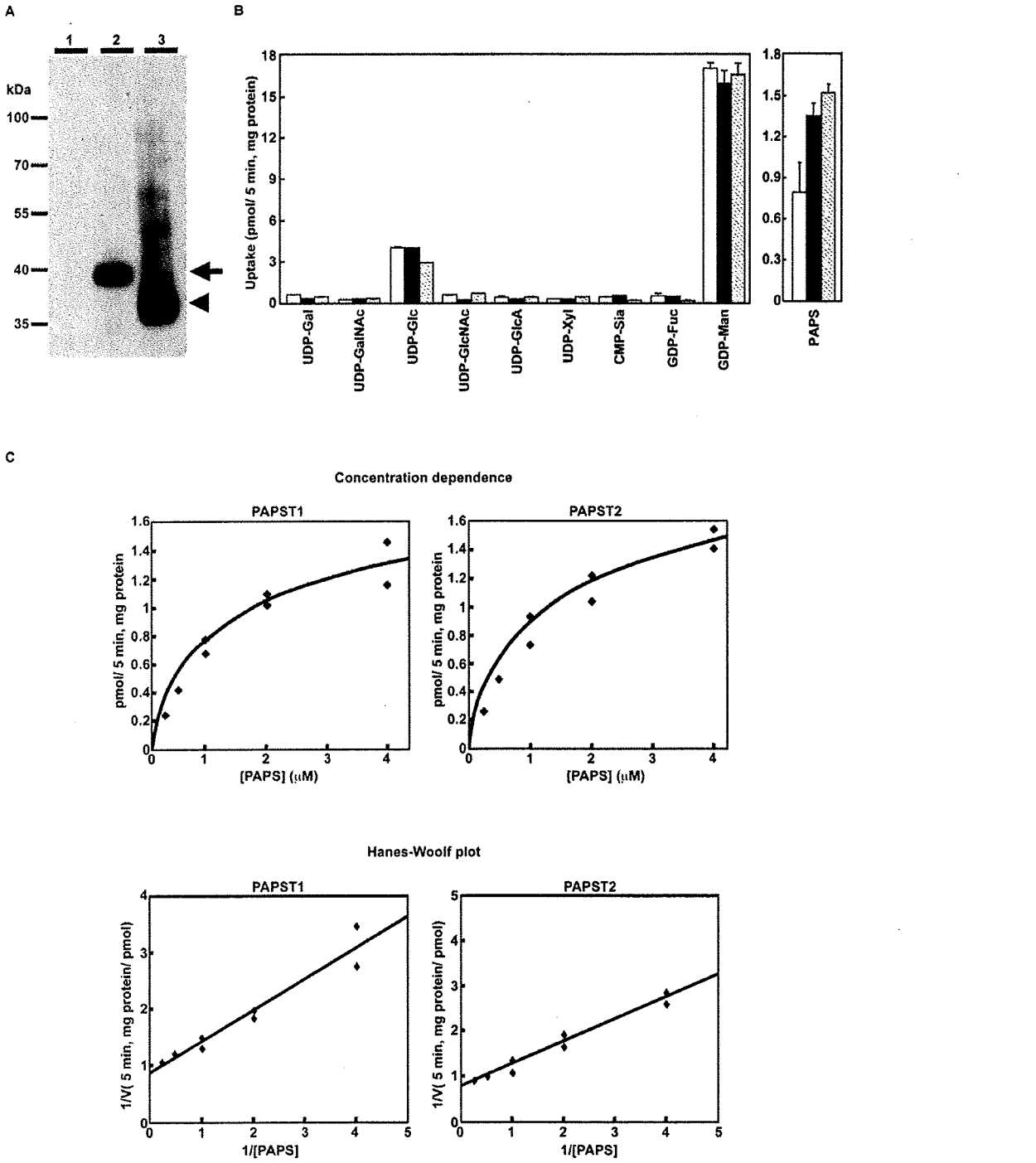

Figure 1. Both mouse *PAPST1* and *PAPST2* encode PAPS transporter proteins. (A) Expression state of PAPST1 and PAPST2 proteins in the Golgi-enriched fraction. Western blot analysis of the P100 fractions prepared from yeast cells expressing either the mock vector (*lane 1*), HA-tagged *PAPST1* (*lane 2*) or HA-tagged *PAPST2* (*lane 3*). An aliquot of 5 μg of protein from the control cells and cells expressing HA-tagged *PAPST1* or 0.5 μg of protein from the cells expressing HA-tagged *PAPST2* was loaded. The *arrow* and *arrowhead* indicate HA-tagged PAPST1 and HA-tagged PAPST2, respectively. (B) Substrate specificity of PAPST1 and PAPST2. Each P100 fraction was incubated in 50 μl of reaction buffer containing 1 μM labelled substrate at 32°C for 5 min, and the radioactivity incorporated was measured. The indicated values are the mean±SD obtained from two independent experiments (*open bars*, Mock; *solid bars*, *PAPST1*; *hatched bars*, *PAPST2*). (C) Substrate concentration dependence. Each P100 fraction was incubated in 50 μl of reaction buffer containing different concentrations of [^{35}S]PAPS at 32°C for 5 min, and the radioactivity incorporated was measured. Specific incorporation was calculated by subtracting the value for the mock transfection from each of the values obtained. *Lower panel*, the Hanes-Woolf plot used to determine the *Km* value is shown.
doi:10.1371/journal.pone.0008262.g001

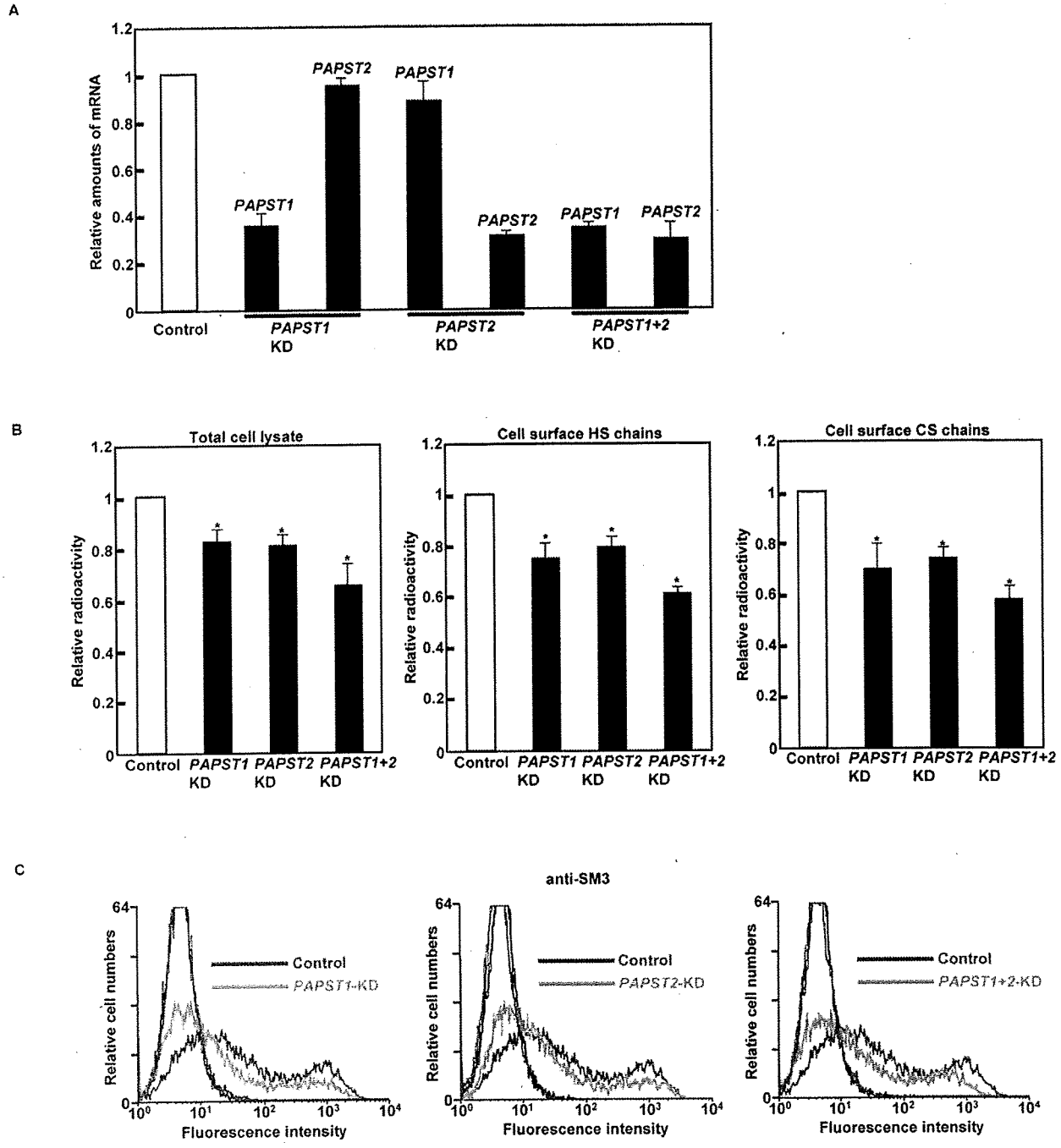

Figure 2. Knockdown of *PAPST1* or *PAPST2* mRNA induced reduction of sulfation in mESCs. (A) Real time PCR analysis of cells 2 days after transfection. Relative amounts of *PAPST* mRNA were calculated after normalization to *β-actin* mRNA in the same cDNA. The results are shown after normalization against the values obtained with control cells (value = 1). The values shown are the means±SD of three independent experiments. (B) Metabolic labeling analysis. The results of total sulfate incorporation into cellular proteins and sulfate incorporation into cell surface HS and CS chains are shown after normalization against the values obtained with control cells (value = 1). The values shown are the means±SD of three independent experiments and significant values are indicated; *$P<0.01$, in comparison to the control. (C) FACS analysis of cells 3 days after transfection using an anti-SM3 antibody (black and blue lines represent the IgM isotype control for control and *PAPST*-KD cells, respectively). Three independent experiments were performed and representative results are shown.
doi:10.1371/journal.pone.0008262.g002

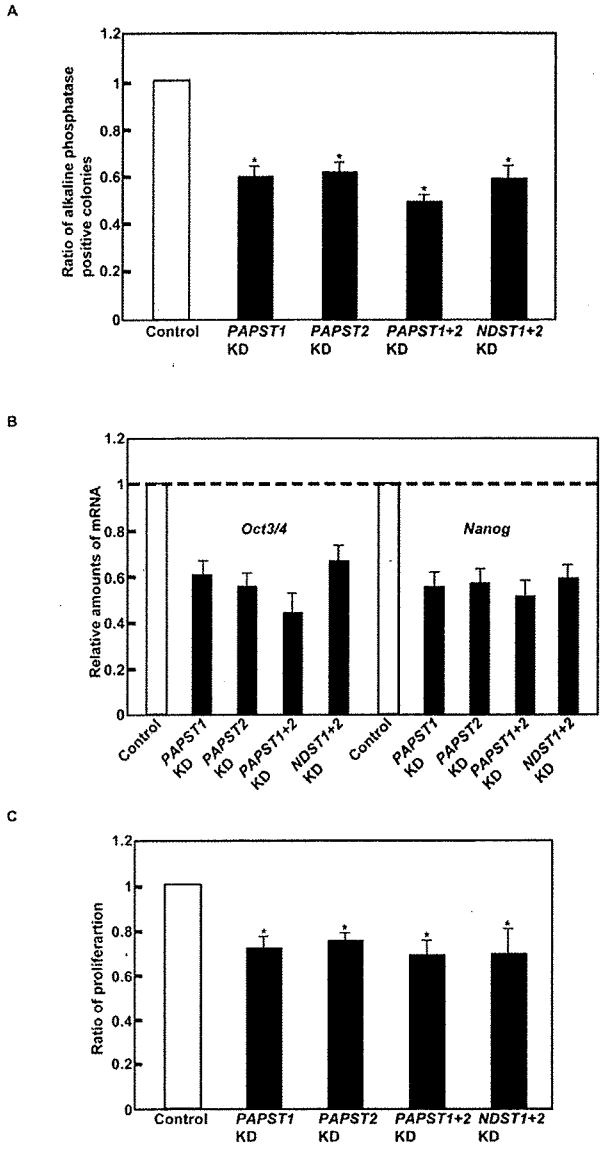

Figure 3. Both *PAPST1*- and *PAPST2*-KD cells showed decreased potential for self-renewal and proliferation. (A) Self-renewal assay. The ratio of alkaline phosphatase positive colonies is shown after normalization against the ratio obtained with control cells (value = 1). Approximately 70% of the colonies derived from the control cells remained in an undifferentiated state in feeder-free culture. The values shown are the means±SD from three independent experiments and significant values are indicated; *$P<0.01$, in comparison to the control. (B) Real time PCR analysis of undifferentiated state markers in the cells 4 days after transfection. The results are shown after normalization against the values obtained for control cells (value = 1). The values shown are the means±SD from two independent experiments. (C) Proliferation assay. The ratio of proliferation 48 h after culture is shown after normalization against the values obtained with control cells (value = 1). The values shown are the means±SD from three independent experiments and significant values are indicated; *$P<0.01$, in comparison to the control.
doi:10.1371/journal.pone.0008262.g003

Therefore, we performed western blotting to determine whether the reduced sulfation affected the signal transduction. We observed a similar increase in the level of phosphorylated STAT3 in control and *PAPST*-KD cells after exposure to LIF (Figure 4A), which shows that sulfation is not required for LIF/STAT3 signaling. Depletion of CS chains by treatment with ChABC also had no effect on LIF/STAT3 signaling (Figure 4B). The levels of Smad1 phosphorylated in response to BMP4 and of ERK1/2 phosphorylated in response to basic FGF (bFGF) or FGF4 were reduced in *PAPST*-KD cells compared to those observed in control cells (Figure 4A). Depletion of CS chains by ChABC treatment had no effect on either BMP4 or FGF signaling (Figure 4B), whereas HS chains were involved in these signaling pathways in mESCs (Figure 4B and [17]). Defects in BMP4 and FGF signaling were also observed in *NDST1+2*-KD cells (Figure 4B). These results suggest that the reduction in BMP4 and FGF signaling in *PAPST*-KD cells was caused by reduced HS chain sulfation.

To date, LIF, Activin/Nodal and bFGF have been reported to contribute to mESC proliferation [7,8,46,47]. It is well known that FGF signaling mediated by HS chains contributes to the proliferation of various types of cell [33]. Thus, we considered the possibility that autocrine/paracrine FGF signaling mediated by HS chains is involved in mESC proliferation. RT-PCR analysis showed that both R1 and E14TG2a cell lines expressed several *FGFs* and *FGF receptors* (*FGFRs*) (Figure S4A). Furthermore, the proliferation of mESCs treated with SU5402, an inhibitor of FGFR1 tyrosine phosphorylation, was reduced compared to that of control cells (Figure S4B), demonstrating that autocrine/paracrine FGF signaling mediated by FGFR1 contributes to mESC proliferation. Therefore, these results suggest that the reduced proliferation of *PAPST*-KD cells (Figure 3C) is due to a reduction in autocrine/paracrine FGF signaling, which in turn is caused by reduced HS chain sulfation (Figure 4A).

Previously, we reported that autocrine/paracrine Wnt/β-catenin signaling occurs in mESCs and that this signaling is regulated by HS chains [17]. We examined Wnt/β-catenin signaling using a luciferase reporter system and found a significant decrease in luciferase activity in both *PAPST1*-and *PAPST2*-KD cells compared to that in control cells (Figure 4C). Furthermore, we confirmed by western blotting that nuclear accumulation of β-catenin was reduced in both *PAPST1*-and *PAPST2*-KD cells compared to that in control cells (Figure S5). Depletion of CS chains by ChABC treatment did not affect luciferase activity in mESCs (Figure S3C). Depletion of HS chains using heparitinase reduced the amount of GSK3β that was phosphorylated in response to Wnt3a, whereas depletion of CS chains by ChABC treatment had no effect (Figure 4B). *NDST1+2*-KD cells exhibited a significant decrease in luciferase activity (Figure 4C). Thus, these results suggest that the reduction of Wnt/β-catenin signaling in *PAPST*-KD cells is caused by reduced HS chain sulfation.

Furthermore, the knockdown of both *PAPST1* and *PAPST2* had an additive effect on Wnt/β-catenin signaling, which suggested that the additive effect of *PAPST1* and *PAPST2* knockdown on self-renewal (Figure 3A and B) could be caused by this additional decrease in the level of signaling.

Taken together, the above results demonstrate that both PAPST1- and PAPST2-dependent sulfation regulates BMP/Smad, FGF/ERK and Wnt/β-catenin signaling in mESCs and suggest that the reduction in signaling is due to reduced sulfation of HS chains, not CS chains.

The Reduction of Sulfation Induces Abnormal Differentiation into Three Germ Layers during EB Formation in mESCs

To determine further contribution of PAPST-dependent sulfation to differentiation of mESC, we examined the *in vitro* differentiation of *PAPST*-KD cells into EBs, which comprise the

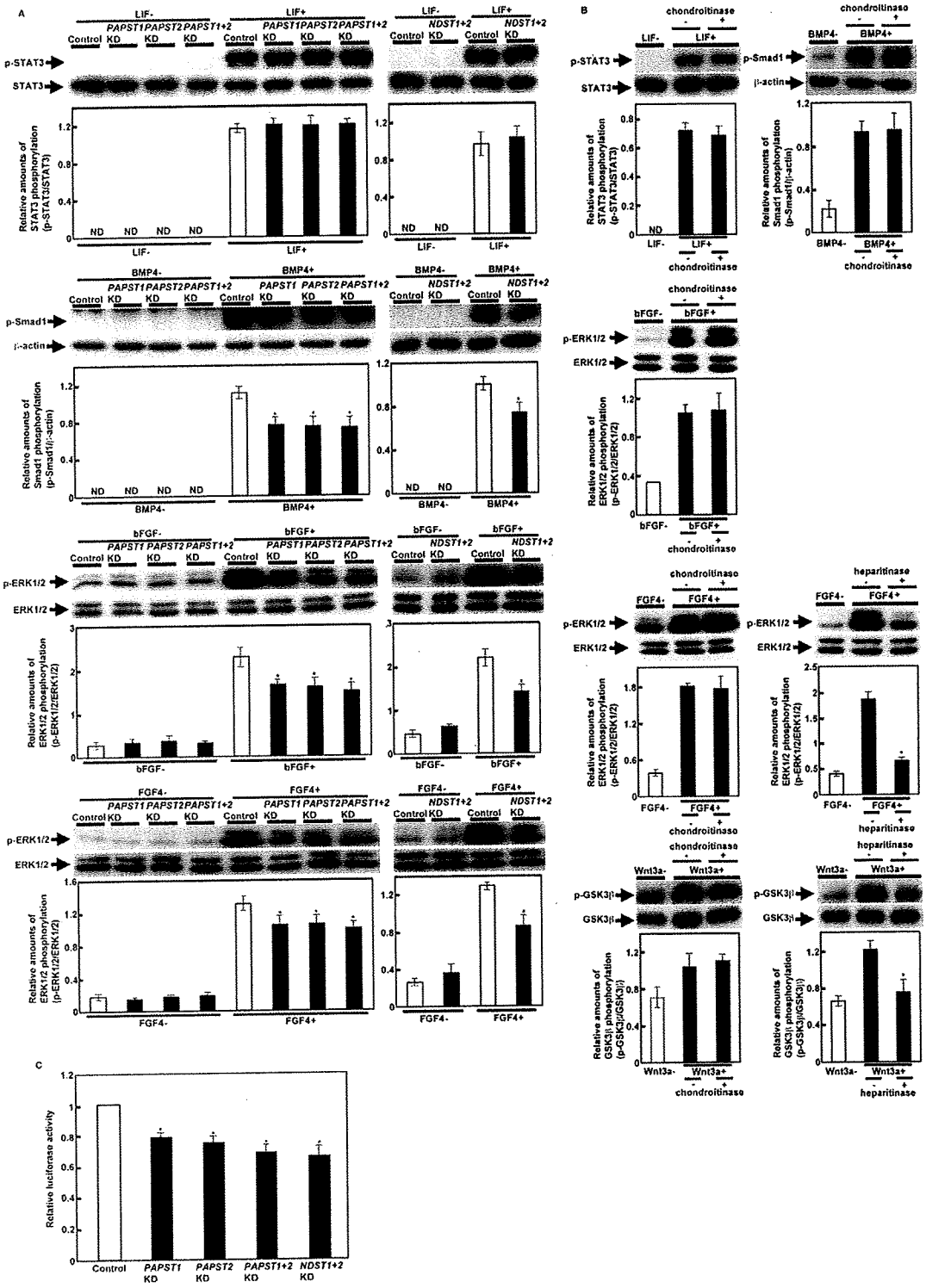

Figure 4. Signaling by specific factors was decreased in *PAPST*-KD cells, but not in CS chain-depleted cells. (A) and (B) Western blot analysis of cells stimulated with the extrinsic factors. Cell lysate was prepared as described in Materials and Methods. Two independent experiments were performed and representative results are shown. The histograms show mean densitometric readings±SD of the phosphorylated protein/loading controls. Values were obtained from duplicate measurements of two independent experiments and significant values are indicated; *$P<0.05$, in comparison to the stimulated control; ND, not detected. (C) Luciferase reporter assay. Relative luciferase activities (TOPFLASH/FOPFLASH) are shown as means±SD from three independent experiments after normalization against the values obtained with control cells (value = 1), and significant values are indicated; *$P<0.05$, in comparison to the control.

doi:10.1371/journal.pone.0008262.g004

three germ layers, endoderm, mesoderm and ectoderm. To maintain the knockdown effects during long culture periods for EB formation, we used stable *PAPST*-KD cells. Control cells were stably transfected with *enhanced green fluorescent protein* (*EGFP*) siRNA expression vectors. Before EB formation, both *PAPST1*- and *PAPST2*-KD cells showed an approximately 50% reduction in *PAPST1* and *PAPST2* mRNA, respectively, as compared to control cells. Then we examined the expression of several germ layer markers by real time PCR 4, 8 and 12 days after EB formation (Figure 5). The expression of neurectoderm markers (*Mash1*, *Pax6*) increased in a time-dependent manner and the expression in *PAPST*-KD cells was higher than in control cells, indicating that neurectodermal differentiation was promoted in *PAPST*-KD cells. The expression of early mesoderm markers (*Brachyury*, *Goosecoid*) and a primitive ectoderm marker (*Fgf5*) decreased in a time-dependent manner and the expression in *PAPST*-KD cells was lower than in control cells, indicating that primitive ectodermal and mesodermal differentiations were inhibited in *PAPST*-KD cells. The expression of ExE lineage markers (*Gata6*, *LamininB1* and *Bmp2*) initially increased and reached a maximum level 8 days after EB formation, after which it decreased. The expression of these genes was lower in *PAPST*-KD cells than in control cells, indicating that endodermal differentiation was decreased in *PAPST*-KD cells. These results indicate that the *in vitro* differentiation of *PAPST*-KD cells is abnormal and that both PAPST1- and PAPST2-dependent sulfation contributes to differentiation of mESCs.

The Reduction of Sulfation Promotes Neurogenesis

The results shown in Figure 5A indicated that *PAPST1* or *PAPST2* knockdown promoted the differentiation of mESCs into neurectoderm. Therefore, we investigated the neural differentiation of *PAPST*-KD cells. We examined the expression of neural differentiation markers by real time PCR 8 days after EB formation (Figure 6A). The expression of several neural markers, such as neural stem/progenitor cell markers (*Nestin*, *Musashi-1*) and proneural markers (*Mash1*, *Math1*, *NeuroD1* and *NeuroD2*), in *PAPST*-KD cells was higher than in control cells in both the presence and absence of all-trans retinoic acid (RA), indicating that the larger amounts of neural stem/neural progenitor cells and neural precursor cells existed in *PAPST*-KD cells. We examined further the ability of *PAPST*-KD cells to differentiate into neurons 6 days after replating EBs. Immunocytochemical staining showed that *PAPST*-KD cells appeared to generate dense networks of neurite outgrowths as compared to control cells in either the presence or the absence of RA (Figure 6B). We confirmed by western blotting that the level of βIII-Tubulin in *PAPST*-KD cells was quantitatively higher than that in control cells (Figure S6). Furthermore, FACS analysis showed that βIII-Tubulin positive cells were more abundant in *PAPST*-KD cells than in control cells (non-treated control, 7.7±3.0%; non-treated *PAPST1*-KD, 18.4±2.9%; non-treated *PAPST2*-KD, 19.4±1.2%; RA-treated control, 24.3±2.4%; RA-treated *PAPST1*-KD, 39.0±4.9%; RA-treated *PAPST2*-KD, 38.1±4.4%), which confirmed that differentiation into neurons was promoted in *PAPST*-KD cells (Figure 6C). These results demonstrate that both PAPST1- and PAPST2-dependent sulfation contributes to the neurogenesis of mESCs.

PAPST-Dependent Sulfation of Both HS and CS Chains Regulates Several Signaling Pathways Required for the Correct Differentiation of mESCs during EB Formation

Several signaling pathways, such as BMP, FGF and Wnt, play important roles in the mouse embryo during early embryogenesis and mESC differentiation [20]. Thus, we examined whether

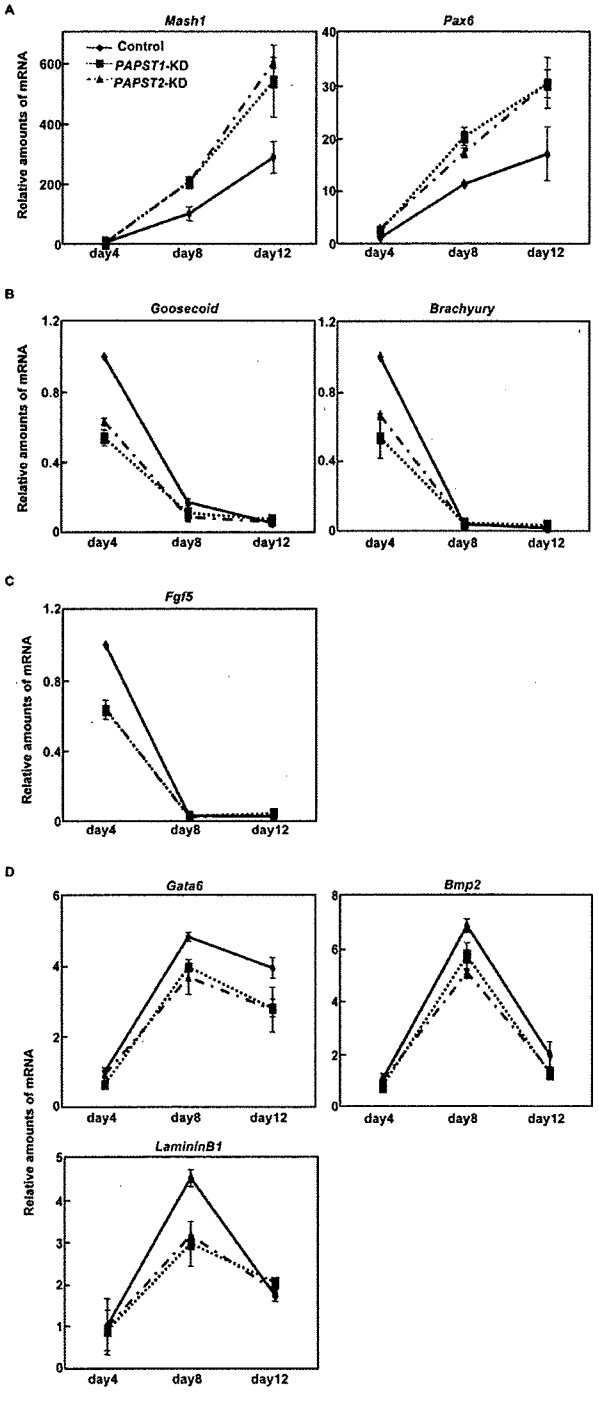

Figure 5. Abnormal differentiation was observed in *PAPST*-KD cells during EB formation. (A)–(D) Real time PCR analysis of germ layer markers 4, 8, and 12 days after EB formation (*A*, neurectoderm marker; *B*, mesoderm marker; *C*, primitive ectoderm marker; *D*, extraembryonic endoderm (ExE) marker). The results are shown after normalization against the values obtained with control EBs on day 4 (value = 1). The values shown are the means±SD of two independent experiments.
doi:10.1371/journal.pone.0008262.g005

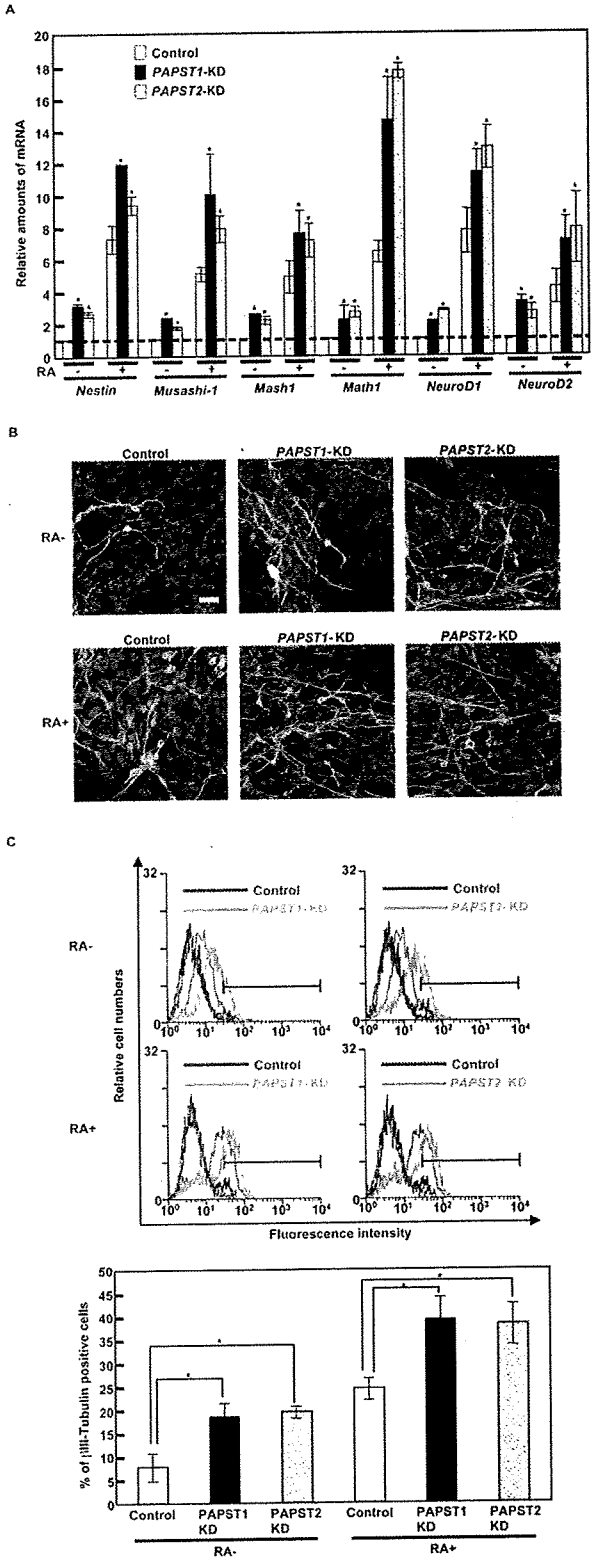

Figure 6. Neurogenesis was promoted in *PAPST*-KD cells. (A) Real time PCR analysis of neural differentiation markers 8 days after EB formation. The results are shown after normalization against the values obtained with control cells not treated with RA (value = 1). The values shown are the means±SD of duplicate measurements from two independent experiments and significant values are indicated; *$P<0.05$, in comparison to the control. (B) Immunocytochemical staining 6 days after replating of EBs. Representative confocal images from two independent experiments are shown. (βIII-Tubulin, green; PI, purple). Scale bar, 20 μm. (C) FACS analysis 6 days after replating of EBs using an anti-βIII-Tubulin antibody (black and blue lines represent the IgM isotype control for control and *PAPST*-KD cells, respectively). Three independent experiments were performed and representative results are shown. The histograms show the ratio of the mean fluorescent intensity within area of the insetted bar representing βIII-Tubulin positive cells to the mean fluorescent intensity over the total area±SD of three independent experiments and significant values are indicated; *$P<0.01$, in comparison to the control.
doi:10.1371/journal.pone.0008262.g006

defects in these signaling pathways contribute to the abnormal differentiation of *PAPST*-KD EBs, especially the promotion of neurogenesis. We performed western blotting of BMP, FGF and Wnt signaling molecules in control and *PAPST*-KD cells 8 days after EB formation. As shown in Figure 7A, the nuclear accumulation of β-catenin and the levels of phosphorylated ERK1/2 and Smad1 were reduced in *PAPST*-KD cells as compared to control cells, which indicated that Wnt/β-catenin, FGF/ERK and BMP/Smad signaling were reduced in *PAPST*-KD EBs. Furthermore, Wnt/β-catenin, FGF/ERK and BMP/Smad signaling were reduced in EBs depleted for HS and CS chains in the absence of RA (Figure 7B). In EBs treated with RA, HS chain depletion reduced signaling via all these pathways as compared with untreated EBs. In contrast, CS chain depletion reduced FGF/ERK and BMP/Smad signaling to a similar extent as HS chain depletion but promoted Wnt/β-catenin signaling (Figure 7B).

To date, K_D values have been determined for the binding of FGFs (e.g., bFGF and FGF4) to HS chains and to CS-E (GlcAβ1–3GalNAc(4,6-SO_3)), a particular form of CS chain [48,49]. Although the binding of BMP4 to HS chains has been demonstrated [50], the K_D value has not been determined. In addition, the binding of BMP4 to CS chains has not been demonstrated. Therefore, we performed surface plasmon resonance (SPR) analysis for Wnt3a and BMP4 against heparin, a structural analogue of HS chains, and CS-E. BMP4 bound to both heparin and CS-E ($K_D = 69.4$ nM and 30.0 nM, respectively) (Table 1). Wnt3a also bound to both heparin and CS-E, as described in other recent reports [51] ($K_D = 26.0$ nM and 27.3 nM, respectively) (Table 1). Thus, it was clearly shown that the sulfate groups of HS and CS chains contribute to the binding of Wnt3a and BMP4 to both HS and CS chains.

These results demonstrate that both PAPST1- and PAPST2-dependent sulfation regulates BMP/Smad, FGF/ERK and Wnt/β-catenin signaling during EB formation and indicate that this regulation is presumably dependent on both HS and CS chains. In addition, the results demonstrate that the reduction in signaling contributes to the abnormal differentiation of *PAPST*-KD cells, such as promotion of neurogenesis.

Discussion

Until now, the functional roles of sulfation during early embryogenesis and in ESCs have not been described well. Here, we demonstrate that both PAPST1- and PAPST2-dependent sulfation is important for extrinsic signaling pathways, such as BMP/Smad, FGF/ERK and Wnt/β-catenin, in both undifferentiated and differentiated mESCs. In the undifferentiated state, sulfation of HS chains contributes mainly to the maintenance of

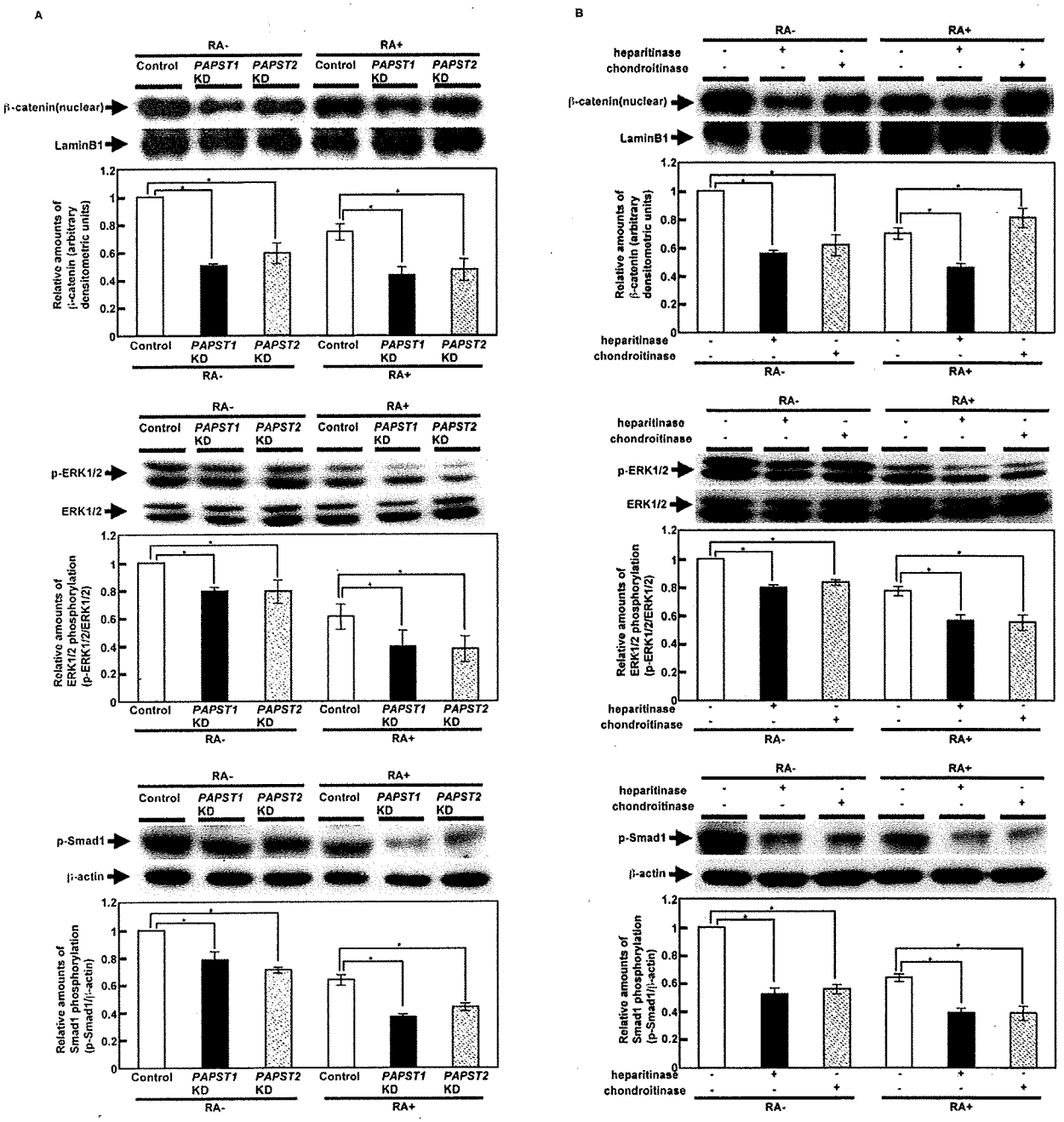

Figure 7. Signaling via a number of pathways was decreased in *PAPST*-KD cells during EB formation. (A) Western blot analysis of several signaling molecules in EBs on day 8. Two independent experiments were performed and representative results are shown. The histograms show mean densitometric readings±SD of β-catenin or the phosphorylated proteins/loading controls after normalization against the values obtained with control cells not treated with RA (value = 1). Values were obtained from duplicate measurements of two independent experiments and significant values are indicated; *$P<0.01$, in comparison to the control. (B) Western blot analysis of several signaling molecules in EBs on day 8 after heparitinase or chondroitinase treatment. Two independent experiments were performed and representative results are shown. The histograms show mean densitometric readings±SD of β-catenin or the phosphorylated proteins/loading controls after normalization against the values obtained with cells not treated with RA and enzyme (value = 1). Values were obtained from duplicate measurements of two independent experiments and significant values are indicated; *$P<0.01$, in comparison to cells not treated with enzyme.
doi:10.1371/journal.pone.0008262.g007

mESCs. During the differentiation of mESCs, namely during EB formation, sulfation of both HS and CS chains contributes predominantly to the normal differentiation of EBs (Figure 8).

Sulfation is an essential modification of carbohydrates and proteins. As shown in Figure 4 and 7, various types of signaling were reduced in *PAPST*-KD cells, presumably due to the reduced

Table 1. The apparent association (k_a), dissociation (k_d) rate constants and equilibrium dissociation constants (K_D) for the interaction of BMP4 and Wnt3a with immobilized heparin or CS-E.

Ligand	GAG	k_a ($M^{-1}Sec^{-1}$)	k_d (Sec^{-1})	K_D (nM)
BMP4	Heparin	2.76×10^{5}	1.92×10^{-2}	69.4
BMP4	CS-E	1.44×10^{5}	4.33×10^{-3}	30.0
Wnt3a	Heparin	2.22×10^{5} [a]	5.77×10^{-3} [a]	26.0 [a]
Wnt3a	CS-E	8.26×10^{5}	2.26×10^{-2}	27.3

The k_a, k_d and K_D values were determined by SPR analysis.
[a]The k_a, k_d and K_D values of Wnt3a against heparin have been published in our previous paper [17].
doi:10.1371/journal.pone.0008262.t001

sulfation of specific carbohydrates and proteins. Two sulfated carbohydrates, HS and CS, were found on the surface of mESCs and EBs ([17] and Figure S7A). We also examined the expression of other sulfated carbohydrates. In mESCs, 3′-sulfo-Le^a, HNK-1 carbohydrate, and sulfatide SM4 were not expressed. The expression level of sulfatide SM3 was low and the reduction of SM3 sulfation in *PAPST*-KD cells was slight. Therefore, we assume that the reduction of SM3 sulfation in the *PAPST*-KD cells is not responsible for the effects observed in this study. However, further studies will be required to elucidate the function of SM3 in mESCs. In EBs, HNK-1 carbohydrate was detected at appreciable levels after induction of neural differentiation by treatment with RA (Figure S7B), whereas 3′-sulfo-Le^a and sulfatides SM3 and SM4 were not detected by FACS analyses in either RA-treated or non-treated EBs (Data not shown). HNK-1 carbohydrate is expressed in the nervous system, including in neural precursor cells [52,53]; however brain development is generally normal in mice in which glucuronyltransferase, which is required for HNK-1 carbohydrate synthesis, has been mutated [54]. Therefore, the contribution of HNK-1 carbohydrate to the neural differentiation of EBs upon RA treatment is considered minor. As mentioned above, the sulfated carbohydrates 3′-sulfo-Le^a, HNK-1 carbohydrate and sulfatides SM3 and SM4 are assumed not to have an important functional role in mESCs and EBs.

The other candidates for sulfation are tyrosine residues on proteins. The sulfation of proteins occurs on specific tyrosine residues as they enter the secretory pathway. However, according to sulfation consensus prediction algorithms (e.g. The Sulfinator) [55], the relevant extrinsic factors, such as Wnt3a, BMP2, BMP4 and several FGFs, are not predicted to be substrates for tyrosine sulfation. This suggests that the reduction in signaling via these pathways in *PAPST*-KD cells is not due to reduced tyrosine sulfation of extrinsic factors. On the other hand, specific sulfated regions of HS and CS chains are required for the binding of extrinsic factors and subsequent signal transduction [41,42,51,56]. Indeed, HS and CS chains contribute to extrinsic factor binding and several signaling pathways in both ESCs and EBs or in EBs, respectively ([17], Figure 4 and 7B and Table 1). These results suggest that the reduction in extrinsic signaling in *PAPST*-KD cells is mainly due to a reduction in HS chain sulfation in ESCs and a reduction in both HS and CS chain sulfation in EBs (Figure 8).

As shown in Fig. 2B, a 30–40% reduction in HS and CS chain sulfation was observed, whereas PAPST activity was reduced by approximately 20%. These substantial effects on HS and CS chain sulfation despite the modest reduction in PAPST activity may be explained as follows. Sulfations of HS and CS chains are modified by several different sulfotransferases. NDST is responsible for the first step of HS chain sulfation and has a key role in determining the sulfated structures of HS chains. The K_m value of NDST1 for PAPS is 40.7 μM [57], whereas PAPST1 and PAPST2 showed relatively low apparent K_m values for PAPS (1.54 μM and 1.49 μM, respectively). Thus, the effect of PAPST1 and PAPST2 can be considered to be significant, because the K_m values of PAPST1 and PAPST2 for PAPS are lower than the K_m value of the sulfotransferase. Therefore, taking into account this assumption, the reduction in HS and CS sulfation can be substantial despite the limited reduction of PAPST activity.

Until recently, it was considered that the pluripotency of mESCs in adherent culture is maintained by a balance among extrinsic signaling pathways, such as LIF, BMP and FGF signaling, and also by a combination of extrinsic and intrinsic factors, such as Oct3/4 and Nanog [4–6,58]. However, we have reported that autocrine/paracrine Wnt/β-catenin signaling through HS chains contributes to the inhibition of mESC differentiation into the ExE lineage by maintaining Nanog expression [17]. In this earlier study, we proposed that proper control of Wnt signaling, in addition to BMP, FGF and LIF signaling, is required for the maintenance of mESC pluripotency. In the present study, we demonstrated that BMP, FGF and Wnt signaling were regulated by the sulfation of HS chains (Figure 8B). Signaling by BMP4, FGFs and Wnts, but not LIF, was disrupted in *PAPST*-KD cells that differentiated spontaneously into the ExE lineage in adherent culture (Figure 4 and S2). Reduction of Wnt signaling induces differentiation into the ExE lineage due to a reduction in the level of Nanog. As reported previously, the level of Oct3/4 expression affects both mESC differentiation and lineage choice [59]. An increase in expression of Oct3/4 of less than twofold causes mESCs to differentiate into primitive endoderm and mesoderm. In contrast, repression of Oct3/4 induces loss of pluripotency and dedifferentiation to trophectoderm. However, as shown in Figure S2, *PAPST*-KD cells differentiated into the ExE lineage, but not into mesoderm or trophectoderm. Hence, the lineage choice of *PAPST*-KD cells may be affected mainly by the reduction in Nanog that occurs due to reduced Wnt signaling rather than by Oct3/4. Furthermore, reduction of FGF4/ERK signaling inhibits differentiation into neural and mesodermal lineages and subsequently induces differentiation into other lineages such as ExE, whereas reduction of BMP signaling induces the neural differentiation of mESCs [23,58,60]. Thus, the spontaneous differentiation of *PAPST*-KD cells into ExE lineage cells is presumably due to a synergetic effect from reduced Wnt and FGF signaling due to reduced HS chain sulfation.

In EBs, signaling by BMP, FGF or Wnt was regulated by sulfation of both HS and CS chains and sulfation of these GAG chains regulated the differentiation of EBs (Figure 5, 7B and 8C). As shown in Figure 5C and D, differentiation into ExE lineage cells (including visceral endoderm) and primitive ectoderm was reduced in *PAPST*-KD cells. It has been reported that FGF signaling is required for the normal differentiation of EBs, differentiation of visceral endoderm, and subsequent differentiation of primitive ectoderm [61]. This report supports our proposal that defects in the differentiation of the visceral endoderm and primitive ectoderm in *PAPST*-KD cells resulted from a reduction in FGF signaling (Figure 8C). Unlike the control cells, *PAPST*-KD cells failed to differentiate into mesodermal cells during EB formation (Figure 5B), presumably due to defects in BMP, FGF and Wnt signaling that were caused by the reduced sulfation of both HS and CS chains (Figure 7 and 8C). This notion is supported by the finding that mesodermal differentiation is induced by BMP, FGF and Wnt signaling in mouse embryos and ESCs [20,62].